UNIVERSIDAD AUTÓNOMA DE NUEVO LEÓN

FACULTAD DE INGENIERÍA MECÁNICA Y ELÉCTRICA

SYNTHESIS AND CHARACTERIZATION OF BLACK TiO2 NANOPARTICLES BY PULSED LASER IRRADIATION IN LIQUID

POR

VERÓNICA ANAHÍ ZUÑIGA IBARRA

COMO REQUISITO PARA OBTENER EL GRADO DE MAESTRÍA EN CIENCIAS DE LA INGENIERÍA CON ORIENTACIÓN EN MATERIALES

SEPTIEMBRE, 2019

UNIVERSIDAD AUTÓNOMA DE NUEVO LEÓN

FACULTAD DE INGENIERÍA MECÁNICA Y ELÉCTRICA

SUBDIRECCIÓN DE ESTUDIOS DE POSGRADO

SYNTHESIS AND CHARACTERIZATION OF BLACK TiO2 NANOPARTICLES BY PULSED LASER IRRADIATION IN LIQUID

POR

VERÓNICA ANAHÍ ZUÑIGA IBARRA

COMO REQUISITO PARA OBTENER EL GRADO DE MAESTRÍA EN CIENCIAS DE LA INGENIERÍA CON ORIENTACIÓN EN MATERIALES

SAN NICOLÁS DE LOS GARZA, NUEVO LEÓN, MÉXICO **SEPTIEMBRE, 2019**

UNIVERSIDAD AUTÓNOMA DE NUEVO LEÓN

FACULTAD DE INGENIERÍA MECÁNICA Y ELÉCTRICA

DIVISIÓN DE ESTUDIOS DE POSGRADO

Los miembros del comité de tesis recomendamos que la tesis ***"Synthesis and Characterization of black TiO_2 nanoparticles by pulsed laser irradiation in liquid"*** realizada por la alumna **Ing. Verónica Anahí Zuñiga Ibarra**, matrícula **1563020** sea aceptada para su defensa de tesis como opción al grado de Maestría en Ciencias de la Ingeniería con Orientación en Materiales.

El comité de Tesis

Dr. Sadasivan Shaji
Asesor

Dra. Bindu Krishnan
Revisor

Dra. Maria Isabel Mendivil Palma
Revisor

Dr. Simón Martínez Martínez
Subdirector de Posgrado

Septiembre 2019

Table of content

Acknowledgements

To God, for the grace of living this experience and for allowing me to fulfill this dream.

To my advisor, Dr. Sadasivan Shaji for the opportunity to work in his research group, for his patience, knowledge and support during this stage.

To the Universidad Autónoma de Nuevo León (UANL), Facultad de Ingeniería Mecánica y Eléctrica (FIME) and the Center for Research, Innovation and Development in Engineering and Technology (CIIDIT) for the facilities to the development of this thesis.

To the University Duisburg Essen of Germany, for the facilities for photocatalytic characterization and for giving me the opportunity to be part of the experience aboard.

To the Conejos Nacional de Ciencia y Tecnología (CONACYT), for the financial support required to carry out this project.

Dedications

To my mother Verónica Ibarra Alanis for her immense love, unconditional support, understanding and for the motivation in every step of my life.

To my father Cesar Zuñiga Rodríguez for his love, for his prayers, and unconditional support during my life and this academic challenge.

To my brothers Karina Lizbeth Zuñiga Ibarra and Luis Antonio Zuñiga Ibarra for being my life partners and their great support.

To my grandparents, to my family, to my loved ones who are the engine of my life and who have supported me in the most difficult moments.

To me, for the person I have become, for every effort made to fulfill this dream and the strength in every obstacle to overcome.

Abstract

In this work, we propose the synthesis and characterization of black TiO_2 nanomaterials by pulsed laser irradiation of white TiO_2 powder by using a nanosecond pulsed Nd:YAG laser of wavelength of 532 nm in presence of different liquid media (water, ethanol, isopropyl alcohol, and dimethylformamide (DMF)). An exhaustive research to find an easy, eco-friendly synthesis method to obtain visible absorbing TiO_2 or black TiO_2. The laser irradiation method brings easy sample preparation, no residues, no high vacuum and no high temperature treatments. The black TiO_2 nanoparticles synthesized by a Nd: YAG laser (532 nm, pulsed duration of 10 ns, and frequency of 10 Hz) presented a morphology modification from square edges to spherical nanoparticles revealed by the scanning electron microscopy (SEM). Raman analysis confirmed the phase and X-ray photoelectron spectroscopy (XPS) revealed the composition and their chemical states. X-ray diffraction analysis discovered a change in crystalline structure. The phase transformation of anatase to rutile is identified by X-ray diffraction which is caused by like-melting process which also involve hydrogenation by H^+ species, and promotion of oxygen vacancies to produce layer defects. The optical and electronic properties were also modified, absorbance spectra were shifted to absorb photons in visible region. Photocatalytic activity of these NPs was evaluated by degradation of rhodamine B under green light irradiation. Enhanced photocatalytic activity was observed by the laser irradiated black TiO_2 nanoparticles. The results of this study can lead to formation of stable, non-toxic and abundant visible light absorbing titanium dioxide nanoparticles having applications in various areas including catalysis, electronic, opto-electronic applications.

List of Figures

Figure 3. 2.- Images of black TiO_2 nanopowders.

Figure 3. 4.- Image of X-ray diffraction (XRD) patterns of white TiO_2, and irradiate d samples in DMF, ethanol, isopropyl alcohol and water media at 60 minutes.

Figure 3. 5.- Raman spectra of white TiO_2 and irradiated samples by 45, 60, 75 and 90 minutes in water medium.

Figure 3. 6.- Raman spectra of white TiO_2 and irradiated samples by 60 minutes in water, ethanol, isopropyl alcohol and DMF media.

Figure 3. 7.- Images of XPS high resolution photoelectron spectra of Ti2p for white TiO_2 and irradiated samples by 45, 60, 75 and 90 minutes in water medium.

Figure 3. 8.- Images of XPS high resolution photoelectron spectra of O1s for white TiO2 and irradiated samples by 45, 60, 75 and 90 minutes in water medium.

Figure 3. 9.- Images of derivates of XPS high resolution photoelectron spectra of Ti2p for the synthesized black TiO_2 in water medium.

Figure 3. 10.- Images of derivates of XPS high resolution photoelectron spectra of O1s for the synthesized black TiO_2 in water medium.

Figure 3. 11.- Images of XPS high resolution photoelectron spectra of Ti2p for white TiO_2 and irradiated samples in DMF, ethanol, isopropyl alcohol and water media for 60 min of irradiation.

Figure 3. 12.- Images of XPS high resolution photoelectron spectra of O1s for white TiO_2 and irradiated samples in DMF, ethanol, isopropyl alcohol, and water media for 60 min of irradiation.

Figure 3. 13.- Images of derivates of XPS high resolution photoelectron spectra of Ti 2p for white TiO_2 and irradiated samples in DMF, ethanol, isopropyl alcohol, and water media for 60 min of irradiation.

Figure 3. 14.- Images of derivates of XP high resolution photoelectron spectra of Ti 2p for white TiO_2 and irradiated samples in DMF, ethanol, isopropyl alcohol, and water media for 60 min of irradiation.

Figure 3. 15.- Valence band Images of white TiO_2 and irradiated samples by 45, 60, 75 and 90 min in water.

Figure 3. 16.- Valence band Images of white and black TiO_2 synthetized in DMF, Ethanol and Isopropyl alcohol media for 60 minutes of laser irradiation

Figure 3. 17.- Chemical state mapping for Water 60, Ethanol 60, Isopropyl 60 and DMF 60.

Figure 3. 18.- Chemical state mapping images of Ti2p and O1s of white and black TiO_2 synthetized in DMF, Ethanol and Isopropyl alcohol for 60 minutes of laser irradiation.

Figure 3. 19.- SEM images of black TiO_2 synthetized in water medium for 45, 60, 75 and 90 min.

Figure 3. 20.- SEM images of black TiO_2 synthetized in DMF, Ethanol and Isopropyl media by 60 min of laser irradiation.

Figure 3. 21.- Diffuse reflectance (%) spectra of b white TiO_2 and irradiated samples by 45, 60, 75 and 90 min in water.

Figure 3. 22.- Absorbance spectra of b white TiO_2 and irradiated samples by 45, 60, 75 and 90 min in water.

Figure 3. 23.- Absorbance spectra of white and black TiO_2 synthetized in DMF, Ethanol and Isopropyl for 60 min of laser irradiation.

Figure 3. 24.- Indirect Band gap estimation of white TiO_2.

Figure 3. 25.- Direct Band gap estimation of black TiO_2 synthetized in water for 45, 60, 75 and 90 min of laser irradiation.

List of tables

List of abbreviations

NPs – nanoparticles

VB – Valence Band

CB – Conduction Band

Eg – Band gap energy

B.E. – Binding energy

e^- – electrons

h^+ – holes

DMF – Dimethylformamide

XRD – X-ray diffraction

XPS – X-ray photoelectron spectroscopy

SEM – Scanning electron microscopy

R – reflectance

A – Absorbance

NIR – near infrared

LED – Light emitting diode

CHAPTER 1

TITANIUM DIOXIDE: PROPERTIES AND APPLICATIONS

1.1 Titanium dioxide

Titanium dioxide (TiO_2), also known as titanium (IV) oxide, is a semiconductor that appears as a white powder and one of the most promising material for environmental applications in the last decade [1,2] since water splitting was completed by UV absorbance of TiO_2 [3]. Environmental applications such as degradation of organic pollutants is widely used by photocatalysis of TiO_2 [2-10]. Due to its high oxidation, low cost, stability and low toxicity, it is one of the most promising materials for those applications and photo-electrochemical water splitting, organic pollutant degradation, dye-sensitized solar cells [9,10] etc.

It is also one of the most abundant semiconductors in the earth [1,2,8]. Titanium can be presented in around 45 minerals such as anatase, brookite, ilmenite, leucoxene, perovskite, rutile and sphene. About 90% of those minerals is consumed by titanium dioxide (TiO_2) of which it used as white pigment in paints (69%), plastic (25%) paper (5%), and others (1%) such as catalysis, ceramics, coated and textiles, floor covering, printing ink and roofing granules [11].

1.1.1 Principal properties of titanium dioxide for photocatalytic applications

In the present chapter, structural, thermodynamic, optical and electronic properties of TiO_2 are described. These properties are the principal ones for the understanding of photocatalytic activity in TiO_2

nanomaterials. Thereafter, properties for modified TiO_2 are properly analyzed and compared.

1.1.1.1 Structural properties of TiO_2

Titanium dioxide has five polymorphs phases: rutile (tetragonal) the stable phase, two metastable low-pressure phases known as brookite (rhombohedral) and anatase (tetragonal) and two metastable high-pressure phases, TiO_2-II (orthorhombic) and TiO_2-III (hexagonal), which be synthetically obtained under conditions of very high pressure, those phases have extremely high hardness [12-15]. In the present work, we focus on anatase and rutile phases, the structural features of polymorphs phases of TiO_2 play an important role depending on the applications. Anatase and rutile are the most common phases found in nature and both have interesting properties for photocatalytic applications [16,17].

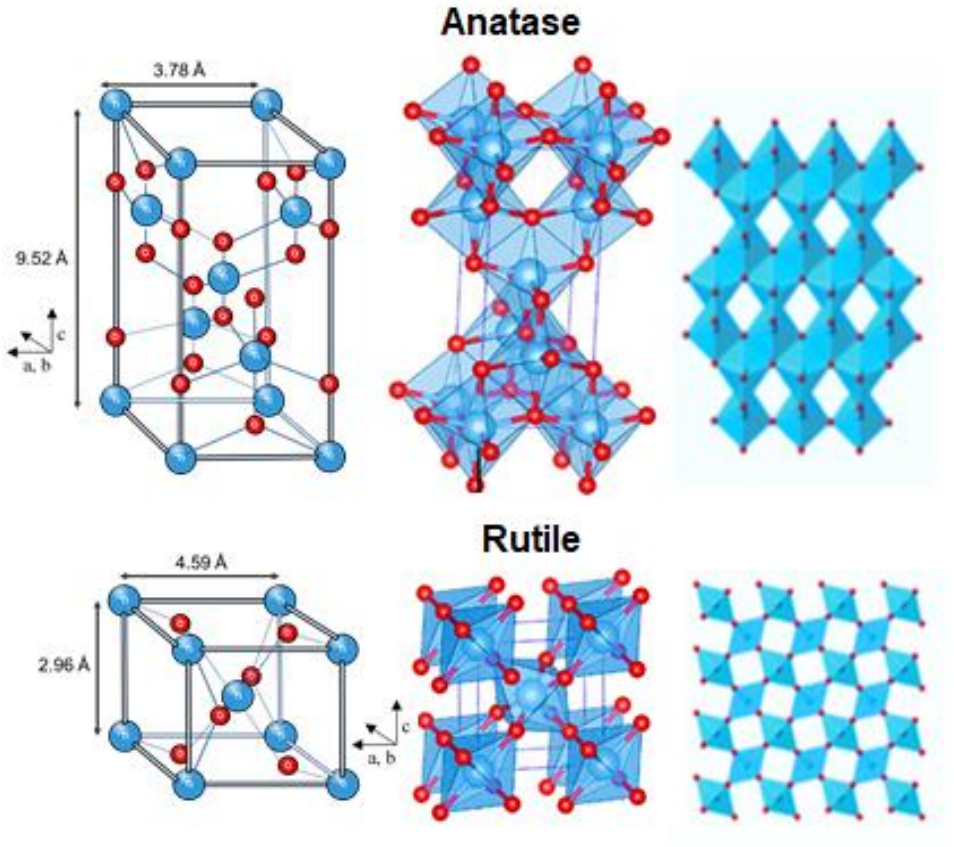

Figure 1.1 Anatase and Rutile crystal phases of TiO_2.

Anatase and rutile have tetragonal crystal structure. The ions Ti^{4+} are around six ions of O^{2-} as octahedral coordination. The distances of Ti-Ti bonds in anatase are greater as rutile but Ti-O distances are smaller as a result of different spatial arrangements of the octahedra (TiO_6). Anatase phase has a zig-zag arrangement and rutile a linear as result, we obtain cis-coordination site for the crystal growth and trans-coordination respectively. [17-18] Lattice parameters of these phases are listed in the Table 1.1, given below.

Table 1.1. Lattice parameters of TiO_x phases.

Phase	Composition	Lattice parameters (nm)		
	at. %O	a	b	c
Rutile	66.667	0.4594	0.4594	0.2959
Anatase	66.7	0.3786	0.3786	0.9517
Brookite	66.7	0.925	0.546	0.516
TiO_2-II	66.7	0.453	0.549	0.491
TiO_2-II	66.7	0.922	0.922	0.5685

Source: J.L. Murray and H.A. Wriedt, 1987

Rutile phase can present a deficit of oxygen, in the present table it is present with a range for those phases (TiO_x to TiO_2) [12]. It is not only known pure anatase phase exhibits more photocatalytic activity as rutile, but also a mixture of anatase and rutile phases increases the activity. Degussa P25 is a mix of 70-80% anatase and 20-30% rutile and it is used to be a reference to compare new photocatalyst due to is high efficiency [16]. Exists the hypothesis that in the interface between anatase and rutile, charges can be trapped, and it delays the recombination process. The structural modeling can be represented as the next figure1.2 [19].

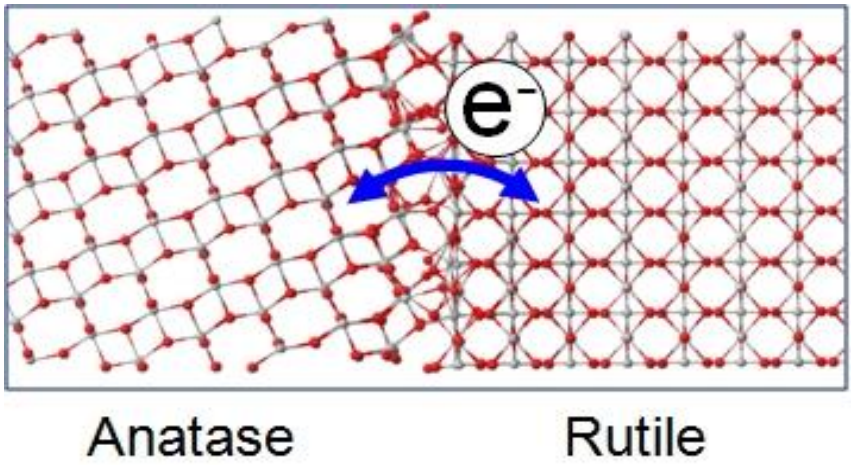

Figure 1. 2. Structural modeling of anatase and rutile phases annealing. Source: Deskins, N. A., Worcester Polytechnic Institute, First Principles Modeling of TiO_2 Rutile/Anatase Interfaces, AIChE Annual Meeting

1.1.1.2 Thermodynamic properties

The study of thermodynamics of polymorphs of TiO_2 is a huge work since TiO_2 exhibits just one stable phase, rutile. Anatase, brookite and rutile phases are the most common phases found in nature, and brookite presents similar properties between anatase and rutile.

Rutile is the only stable phase of all polymorphs of TiO_2. It is shown as a stoichiometric line compound in the phase diagram of titanium (weight percent oxygen vs temperature), figure 1.3. Its compositions vary between 66.6 at. % O to 66.3 at. % O from 1000°C to near the melting point 1870°C, the homogeneity range of rutile TiO_x-TiO_2 is shown in table 1.1 [12].

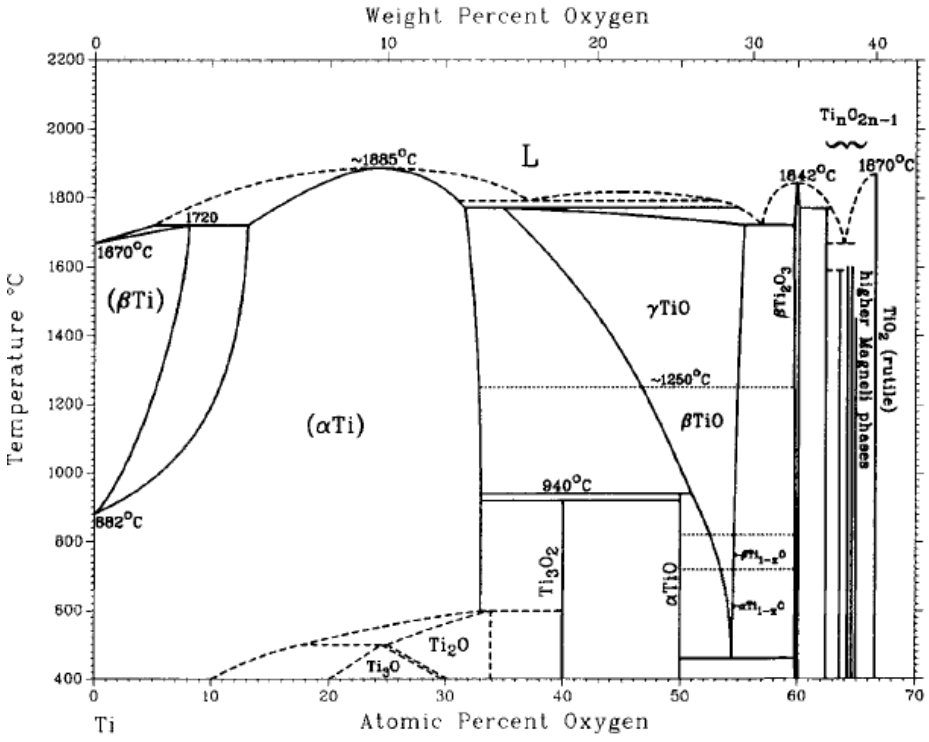

Figure 1.3. Assessed Ti-O Phase Diagram. Source: J.L. Murray and H.A. Wriedt, 1987

Phase transformations result an important concept since crystals phase affects the nanocrystal properties. [16-18] The transformation from anatase to rutile is an irreversible transition as demonstrated. Thermodynamically it cannot be explained since metastable state cannot be defined any specific transition temperature because it has no phase equilibrium [12,17].

Some classical theories also contributed to the understanding of the transition process. The parameters governing the phase transition process (include types of nucleation process and thermodynamic and particle size effects), the phase nucleation depending on solution chemistry, and peptization and growth mechanism for NPs approximate the phase transition understanding [17].

Anatase-rutile transformation occurs around 600-1000 ºC and consists in breakage of Ti—O bonds and a cooperative displacement

helping to the formation of oxygen vacancies and structural rearrangement [17]. The melting point temperature cannot apply for irreversible transitions, however there is a temperature which the atoms move freely and active a melting-like process, that corresponds to the transition from metastable state to stable state [18].

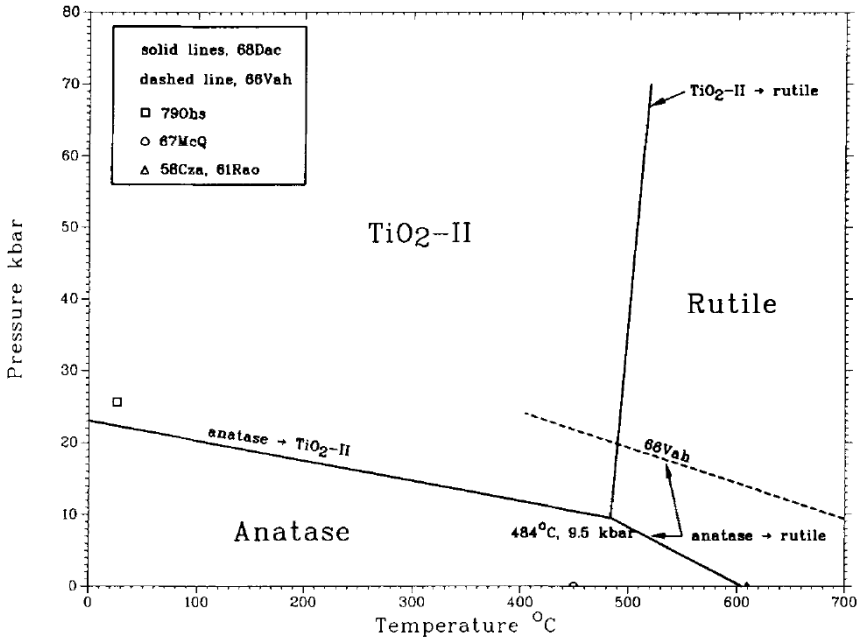

Figure 1.4. Induced Transformation of unstable Anatase and TiO_2-II to Rutile phase. Source: J.L. Murray and H.A. Wriedt, 1987

The nucleation and growth mechanism are the main factors of the anatase-rutile transformation. The synthesis and processing conditions of the materials control the critical nuclei size. Anatase nucleation is inhibited or transformed to rutile during the rutile crystallization. The transformation can be analyzed as two octahedra will be reacting to a third octahedron, which will determine the final crystal structure [18].

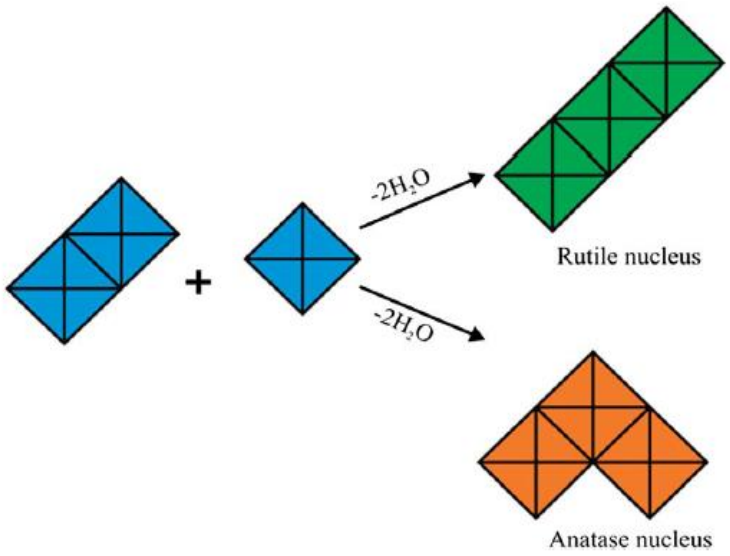

Figure 1.5. Schematic of Anatase-Rutile nucleation reactions between two TiO_6 octahedron.

The rutile nucleation forms a cis-coordination octahedral chains when half of TiO_6 octahedron adjacent to anatase {112} is displaced along the 〈110〉 direction [17]. The high probability for the cis-coordination polymerization is the reason why anatase tends to form easily as the metastable structure [18].

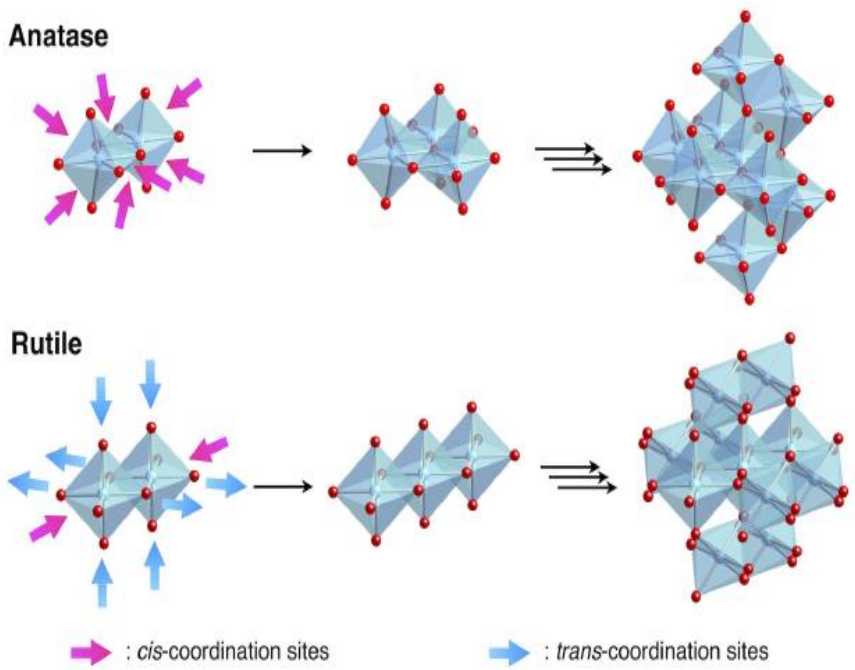

Figure 1.6. Schematic of kinetic and thermodynamic control polymerization of TiO_6 octahedral units as the nucleation of anatase and rutile in TiO_2. [18]

The particle size and surface structure are also observed to influence the phase transformation since thermodynamic stability is size dependent contributed by the bulk balance and surface structure, which occur crystal growth reactions. Anatase has a lower surface and higher bulk Gibbs energy compared to rutile and it is reported anatase NPs are more thermodynamically stable [17,18].

Environmental factors, for example, anions and solvents can inhibit growth of certain crystal phase and modified the shape of TiO_2 NPs [18]. Ti (IV) species in aqueous solutions react with nucleophilic ligands such as -OH group or H_2O producing chemical species such as $[Ti(OH)_n(H_2O)_{6-n}]^{+}_{(4-n)}$. The use of complexing precursors leads a polymorph, it can be observed by pH difference. [17-18]

1.1.1.3 Optical and electronic properties

The optical and electronic properties are one of the most important properties of TiO_2. Depending on the crystal structure, some applications

are preferred. Rutile has a high refractive index, it means it has an effective light scattering phase, reason why it is preferred to performance as filter in solar, pigments and optical communication devices.[17]

The conduction band of TiO_2 consists of 3d orbitals $Ti^{4+,}$ and valence band is formed by an overlapping of 2p orbitals of oxygen [2]. The band gap energy between those bands is 3.2 and 3.0 for anatase and rutile respectively, which means anatase absorption is at 385 nm and rutile at 405 nm in the electromagnetic spectrum.

Although rutile has a lower energy band gap, anatase is preferred to be used in photocatalysis and photovoltaics due to its redox potential. Anatase redox potential is presented and both bands, thus its conduction band is enough positive to oxide hydroxide and its valence band is enough to reduce the oxygen or organic compounds [16].

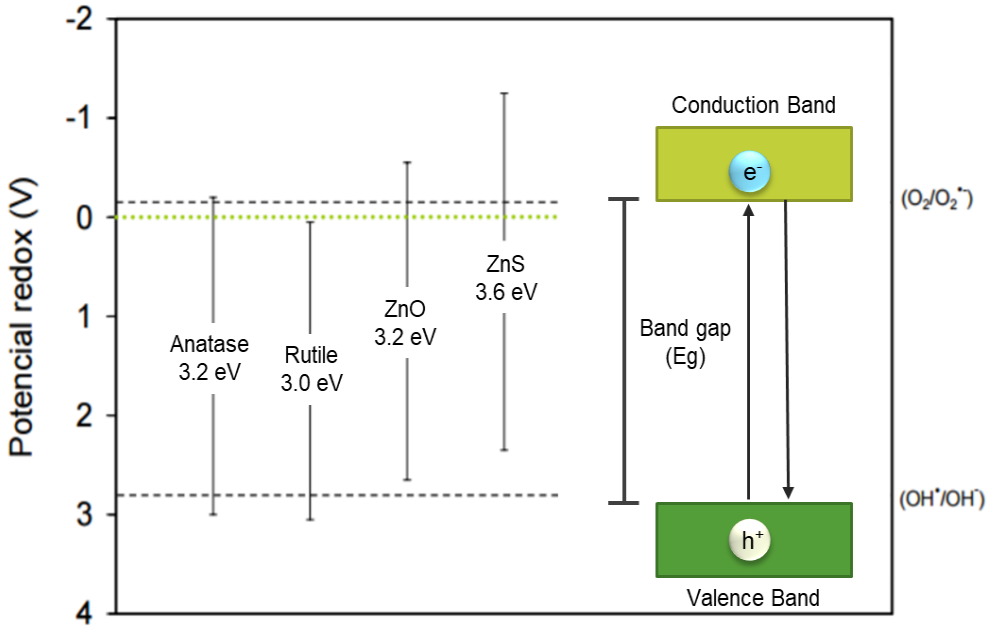

Figure 1.7. Redox potential of some semiconductors and their bandwidth. Source: Raquel Portela, 2008.

The electronic structure plays an important role in photocatalytic process due to the bandgap properties and surface band alignments of

the present phases. Molecular adsorption, defects, particle size, dielectric environment which contribute to the surface state and bring an explanation of the electronic and optical properties of TiO_2[19-21]. In addition, crystallographic orientation also shown different photocatalytic activities [22]. Although anatase is preferred in photocatalytic applications, the mix of anatase and rutile has shown more photocatalytic response [19-22].

The rutile (110) and anatase (101) are the most stable surfaces of each phase, which interact to transfer charge carrier. The possible band edge positions can be described by the next schematic.

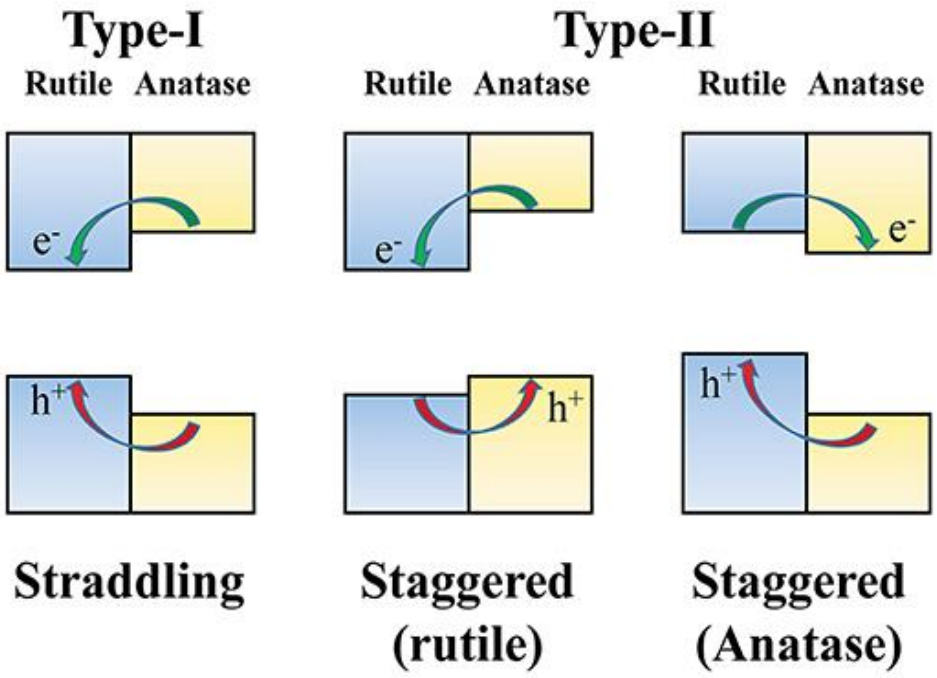

Figure1. 8. Bands annealing between rutile and anatase phase. Type I straddling, electrons and holes anatase travel to rutile phase. Type II staggered by rutile or anatase phase.

There are two types of band alignments, the first one is a straddling type in which valence band and conduction band of rutile phases are located at the anatase band gap region, which provides excited electrons and holes to the valence band and the conduction band of rutile phase.

The type II is staggered and has two configurations, up and down anatase position where electrons and holes are deposited in both phases [20].

1.2 Modified TiO_2

The exhausting search to improve the photocatalytic activity of TiO_2 by its modification requires the reduction of its bandgap to obtain visible light adsorption, getting suitable potential of the valence band (VB) and conduction band (CB) to increase the redox potential of photogenerated radicals, and finally higher mobility of the charge carriers to avoid a fast recombination [2]. The electronic and structural properties of TiO_2 can be modified by cation doping (rare earth metals, noble metals, transition metals and poor metal) [2,9], anion doping such as N, C, F, S) [2-5,9], self-doping [23], coupled semiconductor photocatalysts and dye sensitization organic molecules coated on the TiO_2 surface [2,5]. Optical absorption of is TiO_2 limited to UV region (only 4% of solar radiation) because of the higher bandgap.

1.2.1 Modification routes of titanium dioxide

1.2.1.1 Cation and anion doping

There are two types of doping: cation and anion doping. The responsible of the change in properties by cation doping are the nature and concentration of the dopant, as well as the length and photocorrosion at the surface of the material [25].

The cation doping can be carried out by rare earth metals, noble metals, transition metals, and poor metals. It was found rare earth metals such as cerium (Ce) doped TiO_2 (mixture of anatase and rutile) can increase the specific surface area by retarding the growth of grain size, which allows the adsorption of more reactants and inhibits the recombination of (e^-/h^+) pairs, it is due to the transition of the 4f electrons

[26]. By noble metals doping as well as rare earth metals, an increase of specific surface area was observed which allows to contribute to the separation of photogenerated charge carriers by retarding the recombination [27]. Transition metals have an incomplete d subshell which promote charge-transfer transition with the conduction or valence band. It tunes the electronic structure and shifts light absorption region from UV to visible light and prevents the recombination of photo generated electron-hole pairs [26, 28]. Finally, the poor metals are the post-transition metals such as aluminum (Al), gallium (Ga), indium (In), tin (Sn), thallium (Tl), lead (Pb) and bismuth (Bi) [29]. The doping by bismuth is also observed to trap the electrons and ensure the separation of the charge carriers [26].

As it was mentioned, the cation doped by metals has shown interesting results, as well as the decrease in photocatalytic activities is also reported. The drawbacks such as thermal instability, and metals centers which act as an electron traps are encouraging to the alternative of anionic doping. Recently, more reported researches support the anion doping that has received a great interest [30]. Anion doping by carbon (C), nitrogen (N), sulfur (S) and iodine (I) can improve the morphology, narrow its band gap and minimize the recombination centers but they do not act as charge carriers. Carbon and nitrogen result to exhibit higher photocatalytic activity under visible light irradiation [2, 31]. The incorporation of carbon introduced new states C 2p near to the VB edge to narrow the band gap of TiO_2. Carbon facilitate the absorption of visible light when carbonaceous species are at the surface. On the other hand, nitrogen favors the formation of oxygen vacancies and can simultaneously substitute both oxygen and titanium sites as $Ti_{1-y}O_{2-x}N_{x+y}$ [31]. However, limits on the incorporation of dopant and reduction of photocatalytic activity due to annealing process are some drawbacks of anion doping [26].

1.2.1.2 Coupling of semiconductors

An alternative to overcome the drawback of doping is coupling of two semiconductors. It also mitigates the charge carrier recombination. Some examples of coupled materials are metal oxides as CdS, SnO_2, WO_3, FeO_3 and Bi_2S_3. Although this coupling materials has shown to be a promising alternative for photocatalysis it remains yet limited in water treatments [2].

1.2.1.3 Coating of organic and inorganic dyes

It consists of a surface treatment which involves an organic or inorganic dye attached to TiO_2 surface. The process involves dye molecules are excited under visible light, then photogenerated electrons are transfer to the band conduction [2]. However, loss of coating material and poor conductivity, lack of stability are the major drawbacks.

1.2.1.4 Surface modification

As we already mentioned, band narrowing is a desirable property to improve white TiO_2 nanomaterials. This band narrowing was observed by the introduction of a thin disordered layer surrounded by a core of ordered TiO_2. In addition, the incorporation of the nonmetal element X (X = H, N, S, I) in the oxygen-deficient amorphous layers promote the color change in shell surface material. Modified shell-core TiO_2 is also a promising material structure to photocatalytic or sensible surface applications. [5].

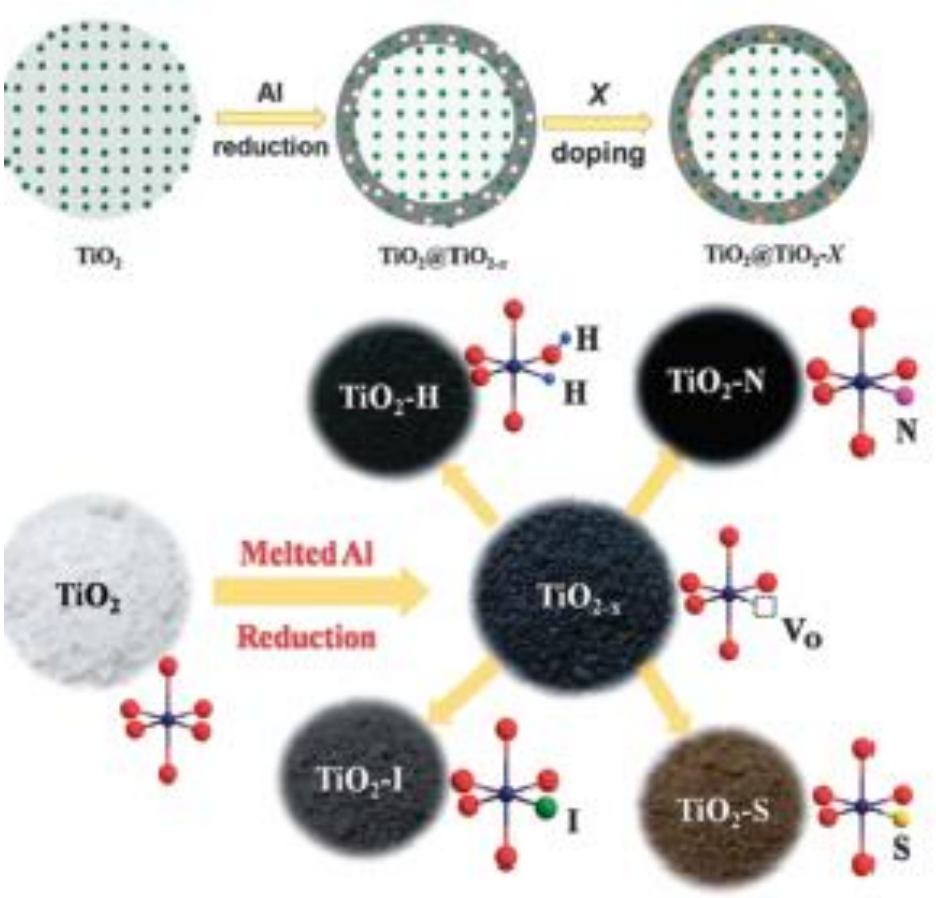

Figure 1.9. Schematic of Anatase-Rutile nucleation reactions between two TiO_6 octahedron.

Recently one of the most promising TiO_2 modification is the surface defect engineering. Those defects are induced due to oxygen vacancies, Ti^{3+} doping or atomic arrangement disorder and those defects diffuse to the surface above 600 °C [25]. The surface disordered layer improves the surface water oxidation kinetics and stability. The conductivity of the disordered surface plays an important role to accelerate charge transport in photo electrochemical applications. Structural defects to decrease the coordination number to improve the electronic structure and catalytic activities [25].

1.2.2. Color change

The modification of TiO_2, whether by doping, coating or surface modification exhibited color change (yellow, brown, gray, blue dark, black) due to the introduction of new band levels [25].

The color change is occasioned by material composition and morphologic composition. Phenomenas such as selective absorption and scattering are caused by material composition are presents due to the material composition, meanwhile surface roughness, Rayleigh scattering, diffraction and interference are due to the morphologic composition [34].

1.3 Black TiO_2

The black color is one of the most attractive materials since black TiO_2 can absorb visible light radiation, and it exhibits band narrowing due to a thin disordered layer as a shell around an ordered-core TiO_2 material [32,33]. The present work is focused on black TiO_2 nanomaterial synthesis and studies on their structure, morphology, composition and optical properties.

In 2011, *Chen et. al*. increased the solar absorption of TiO_2 by shifting white TiO_2 to black TiO_2 using a hydrogen thermal treatment [23]. Since then, the black TiO_2 nanomaterials have become one of the most investigated modification of TiO_2 because of its optical, chemical and electronic properties [5]. These properties allow black TiO_2 to be attractive in photocatalysis, photoelectrochemical sensor, catalysis, lithium-ion rechargeable battery, supercapacitor, field emission, fuel cell and microwave absorption applications [5].

In 2015, Chenyao *et. al.* prepared black hydroxylated TiO_2 nanocrystals by a powerful ultrasonic technic increasing its photocatalytic activity. At the same year, Chen *et. al.* synthetized black TiO_2 nanoparticles by laser irradiation in water [4]. They used this simple preparation using white powder and a laser of 355 nm (Nd: YAG).

More recent, Hui Song *et. al.* found an effective way for formation of oxygen vacancies in black TiO_2 by using ultrathin hollow (sphere) with high crystalline quality, small grain size (~8 nm), and ultrahigh surface area (168.8 $m^2 g^{-1}$) through Al reduction. [34]. Kan Zhang *et. al.* published results on the surface localization of defects in which the study of liquid/solid interface influence the photochemical reactions [25].

1.3.1 Properties of black TiO_2

Properties of black TiO_2 nanomaterials are listed: structural disorder near the surface, presence of Ti^{3+} ions, existence of oxygen vacancies, Ti—H groups, Ti—OH groups, modification of valence band edge and the theoretical consideration of hydrogenated black TiO_2 nanomaterial. In some cases, some or all those properties are a summary of all reported in the case of black TiO_2 nanomaterials [5].

1.3.2 Synthesis of black TiO_2

Black TiO_2 have been synthesized by different methods such as hydrogen thermal treatment, hydrogen plasma, chemical reduction, chemical oxidation, and electrochemical reduction. [4-7] These treatments need high pressures, high temperature treatment for longer durations, some cases with vacuum and even toxic precursors to obtain black TiO_2 [5]. To resolve the environmental problems, eco-friendly synthesis methods are required. The pulsed laser irradiation technique for synthesizing modified nanostructures of TiO_2 is attractive due to its simplicity, less usage of toxic reagents and absence of costly vacuum systems.

1.3.3 Pulsed laser irradiation in liquid

The pulsed laser irradiation in liquid technique is a simple technique to synthesize nanoparticles. It consists in irradiating a sample (metal target or dispersed solid particles) immersed in a liquid (solvent) with a laser beam. The laser heats the sample and melt the surface, the contact with the liquid cold down the particles. Previous studies have shown anatase-rutile transformation and fragmentation phenomenon in post irradiation at 0.23 J/cm^2 of fluency [35].

1.3.3.1 Laser-matter interaction

The laser irradiation phenomenon involves different physical-chemical process by the interaction of electromagnetic radiation and matter. The correlation of those phenomena and matter are connected by the optical and thermal properties of the material and can be classified as: absorption of radiation, thermal conduction, melting phenomena and plasma formation [34].

1.3.4 Applications of black TiO_2 nanomaterials

Black TiO_2 and partially black TiO_2 / modified TiO_2 have some oxygen vacancies, presence of Ti^{3+} ions, structural disorder/defects in the surface, Ti-OH and Ti-H groups, and modifications of the valence band edge [23]. The role of the disorder/defects in TiO_2 is still under debate in order to understand its chemical composition and electronic structure as well as its mechanism in photocatalysis [10,25]. These materials can be also used for photoelectrochemical sensors, catalysis, lithium-ion rechargeable battery, supercapacitor, field emission, fuel cell and microwave absorption applications [5].

1.4 Photocatalytic Process

Photocatalysis process consists of the use of a semiconductor, which produces an electron-hole pair by absorbing a photon of wavelength less than hγ / Eg, where Eg is the bandgap energy. An electron from the valence band (VB) is promoted to the band of driving (CB).

$$TiO_2 + hv \rightarrow e^- + h^+ \qquad \text{(Ec. 1)}$$

(a) oxidation reactions from the photogenerated holes on the valence band and (b) reduction reactions from photogenerated electrons on the conduction band [2]

The valence band hole is strongly oxidant and the electron of the conduction band is moderately reducer. Thus, both species participate in redox reactions. In aqueous systems, the holes can react with the absorbed species and generate reactive radicals:

$$h^+ + H_2O \rightarrow OH^\bullet + H^+ \qquad \text{(Ec. 2)}$$

$$h^+ + OH^- \rightarrow OH^\bullet \qquad \text{(Ec. 3)}$$

Those radicals are highly reactive with most of the organic molecules and many of the inorganic species. The result is an oxidation of the organic compounds and the formation of carbon dioxide, water and inorganic acids. The electrons reduce the O_2 to form a superoxide. The superoxide reduces the possibility of recombination of the electron-hole pair, as well as, generates hydroxyl radicals.

Photocatalytic process involves three crucial steps: light absorption, charge separation in the bulk region, and charge recombination on the surface [25].

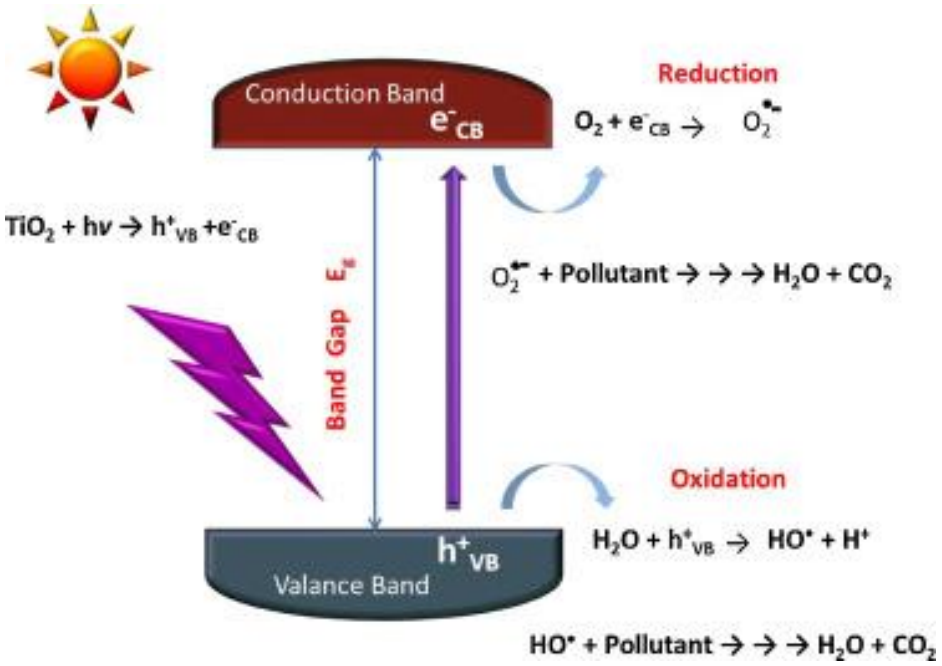

Figure 1. 10. Schematic of general photocatalytic process of TiO_2 with its respective reactions.

1.4.1 Heterogeneous photocatalysis

The heterogeneous photocatalysis belongs to the group of so-called advanced oxidation technologies, together with other processes also in the generation of oxidant radicals. By using photocatalysis processes there are some important considerations:

• Maximum organic concentration of several hundred mg/L. it is not normally a convenient option if they exceed the value of 1 g/L (unless you resort to a previous dilution stage).

• Non-biodegradable contaminants. If the pollutants are not biodegradable, photocatalytic processes can be a valuable alternative. Hazardous pollutants present complex organic mixtures. The main advantages of photocatalysis, its little or no selectivity.

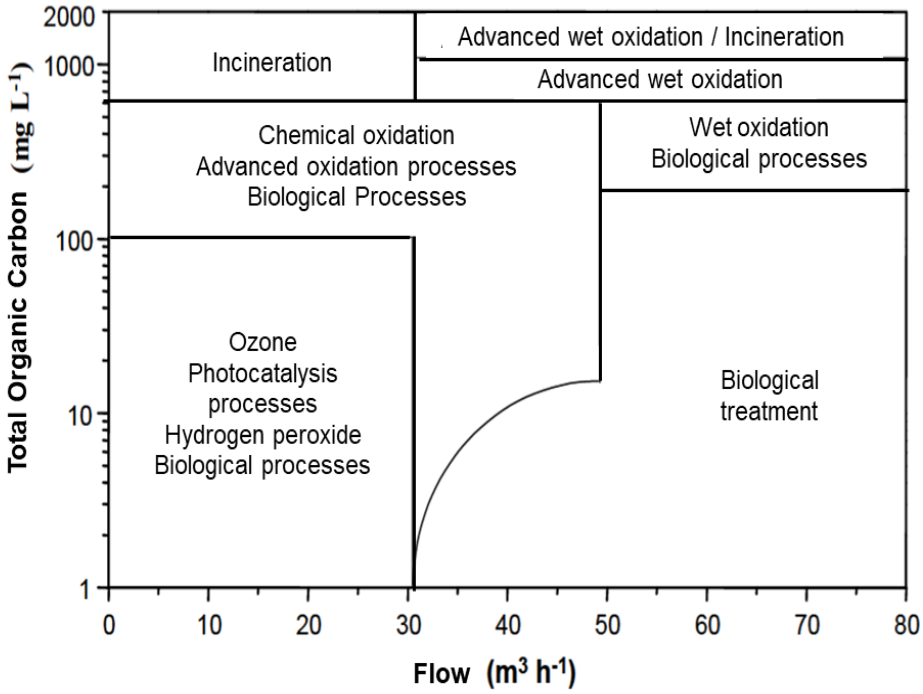

Figure 1.11. Schematic of Anatase-Rutile nucleation reactions between two TiO_6 octahedron.

1.5 Hypothesis

Pulsed laser irradiation at 532 nm (low energy) of white titanium dioxide (TiO_2) in different liquid media (water, DMF, ethanol and Isopropyl alcohol) result in black TiO_2 nanomaterials with different morphologies, optical properties and enhanced photocatalytic activity under visible light.

1.6 Objectives

1.6.1 General Objective

To synthesize and characterize modified black TiO_2 nanomaterials by pulsed laser irradiation (532 nm) of white TiO_2 in different solvents (deionized water, isopropyl alcohol, dimethylformamide and ethanol) to improve the photocatalytic activity by visible light irradiation.

1.6.2 Specific Objectives

- To synthesize black-modified TiO_2 by pulsed laser irradiation of white TiO_2 in deionized water.
- To synthesize black TiO_2 in different organic solvents (isopropyl alcohol, dimethylformamide and ethanol).
- To characterize the crystal structure, morphology, chemical states and optical properties of black TiO_2 nanomaterials.
- To prove the photocatalytic activity of black-modified TiO_2.
- To compare the photocatalytic activity of white TiO_2 vs black TiO_2.

1.7 Scientific contribution

The technique used in this work was successful to synthesize black TiO_2 at low energy irradiation. The laser irradiation by a moderate laser energy and white TiO_2 in different solvents media provided stable black TiO_2 at normal conditions to obtain enough quantity of material. The motivation for the development of the synthesis of black TiO_2 nanomaterials promote research of new properties and new applications not only photocatalysis but also catalysis, solar cells, lithium-ion rechargeable battery, supercapacitor, field emission, fuel cell and microwave absorption applications.

CHAPTER 2

METHODOLOGY FOR THE SYNTHESIS AND CHARACTERIZATION OF BLACK TiO_2

2.1 Synthesis of black TiO_2 by pulsed laser irradiation in liquid

The nanopowders of black TiO_2 were prepared by the laser irradiation of 0.15 g of white TiO_2 powder into 10 mL of the liquid. The white TiO_2 dispersions were prepared in deionized water, ethanol (C_2H_5OH), isopropyl alcohol (C_3H_8O), and dimethylformamide (DMF, C3H7NO) and were ultrasonicated for 15 minutes to obtain a uniform dispersion of the nanopowders (Fig 2.1(a))

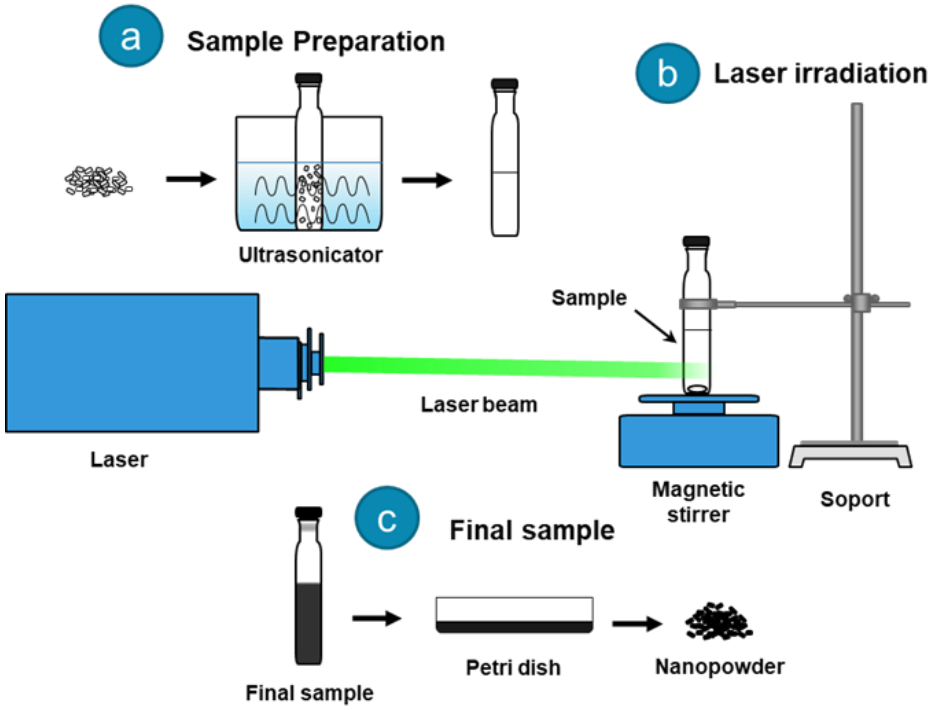

Figure 2.1. Experimental setup for the synthesis of black TiO_2. (a) Sample preparation of the white TiO_2 powder, (b) Schematic of experimental setup of the laser irradiation, (c) Final treatment of the sample to get nanopowders.

The laser irradiation was carried out by a Nd:YAG pulsed laser (λ = 532 nm) with a pulse duration of 10 ns and frequency of 10 Hz during 45, 60, 75 and 90 minutes. The dispersion was continuously agitated during the irradiation. The laser energy was around 350 mJ/pulse in a spot diameter of 1 cm, thus with an estimated fluency of 0.65 J/cm^2. In Fig 2.1 (b) it is shown a schematic of the experimental setup of the laser irradiation.

The samples were dried at room temperature in a petri dish, Fig 2.1 (c), for a period time of 2 to 3 days. Finally, the powder was collected and prepared to characterize, as follow in the next section.

2.2 Characterization of black TiO_2

The crystalline structure, phases present, morphology of the nanomaterials obtained, their elemental composition, chemical states of the elements present, valence band analysis and optical properties of black and white TiO_2 powder were studied by different techniques. Details of these studies with corresponding graphs/images and their observations, findings, results and proper discussions are reported in section 3.

X-ray diffraction (XRD) technique was used to identify the crystal structure and phases present. A Panalytical Empyrean diffractometer with Cu_αX-ray (λ = 1.5406 Å) as irradiation source was operated at 45 kV and 40 mA with a Pixel detector in Bragg-Brentano geometry for the analysis. The scans were performed in the 2θ range from 10 to 100° with a scan step of 0.016° and 20 s per step in continuous mode. Finally, a Rietveld method was employed to determine the lattice parameters and qualitative composition for each phase.

A Thermo Scientific DXR Raman microscope was employed to evaluate the crystal phases identification. By acquiring the vibration

spectra for these nanopowders, changes in their phases and amorphous nature of modified TiO_2 was observed.

X-ray photoelectron spectroscopy (XPS, Thermo Scientific K-alpha) was applied to study the elemental composition and chemical states of the nanoparticles. Mapping studies were carried out to identify Ti1S and O1s states. Differential data analysis of the high resolution photoelectron spectra is also reported in section 3. The spectral analysis was carried out at high vacuum with a charge compensation using a flood gun.

Further, the morphology and particle size of the synthesized nanoparticles were examined by scanning electron microscopy (SEM, Hitachi SU8020).

For the optical properties, the diffuse reflectance was examined by a UV-Vis-NIR spectrophotometer (Jasco 770) to determine the absorbance spectra. It was estimated by the next function A = log(1/R), where R is the diffuse reflectance. Kubelka-Munk method was applied to estimate the energy band gap.

Finally, the photocatalytic activity was analyzed by the degradation of rhodamine B (Fig 2.2 (a)). The solution was prepared by adding 2 mg of photocatalyst in 18 mL of deionized water and 2 mL of rhodamine B (10 mg/L). Before the LED irradiation, the solution was in dark for 1 hour.

The photocatalytic process was performed by the irradiation of green LED (523 nm) with 10W power and a typical flux (lumens) of 1000 mA. The green LED was localized in the bottom of the photoreactor, as shown in Fig 2.2(b). Finally, the experimental configuration for the photocatalysis is shown in the Fig 2.2(c). Online UV (Ocean Optics Spectra Suite) parameters were integration time was 50 milliseconds and scans to average of 60.

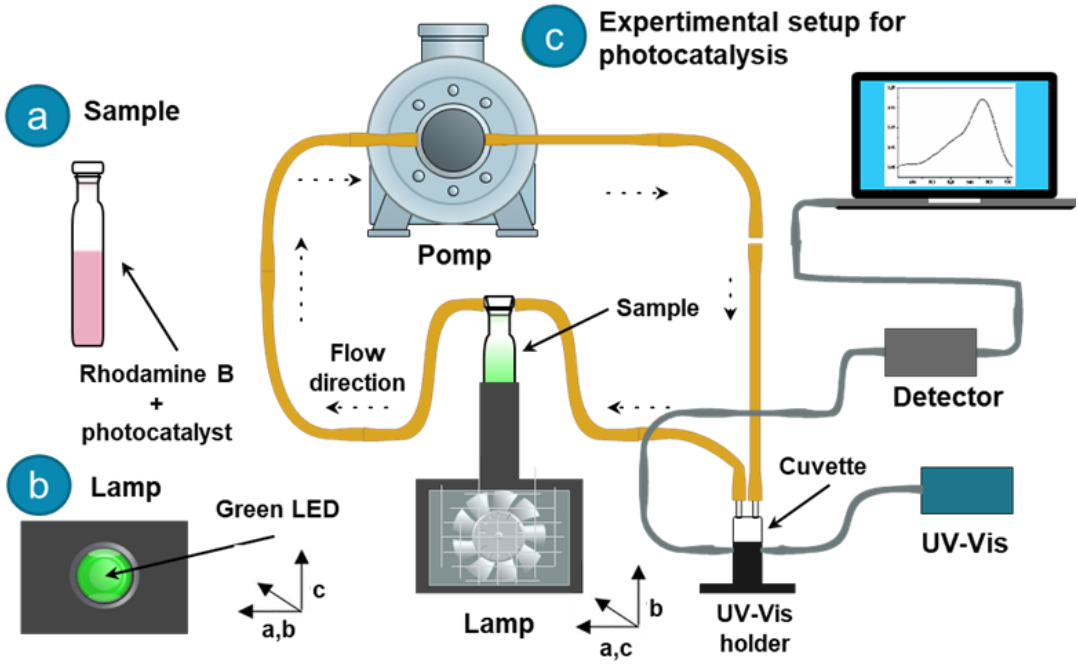

Figure 2.2. Experimental setup for the photocatalysis. (a) Sample preparation of the photocatalytic solution, (b) Schematic of lamp of the photoreactor, (c) Schematic of experimental setup of photocatalysis.

CHAPTER 3

STRUCTURE AND PROPERTIES OF BLACK TiO_2 NANOPARTICLES

3.1 Synthesis of black TiO_2: Water, DMF, Isopropyl alcohol and Ethanol solvents

For the synthesis of black TiO_2 in water, a quantity of 0.15 g of white TiO_2 powders were added to 15 mL of deionized water. The dispersion was ultrasonicated for 15 minutes to obtain uniformity for the colloid and however the solution was agitated by a magnetic stirrer during the irradiation to avoid the particle agglomeration.

The samples were irradiated for different irradiation times - 45, 60, 75 and 90 minutes. During the first 15 minutes of irradiation, the solution turned from white to light gray color, and by time the solution was turning to gray (30 minutes), for 45 minutes the solution had a darker gray color. The partial black color appeared after 60 minutes of irradiation and the solution became thicker through irradiation time. The black color was reached at 75 minutes. The 90-minutes sample resulted in a darker color and a thicker final solution, Figure 3.1 (a).

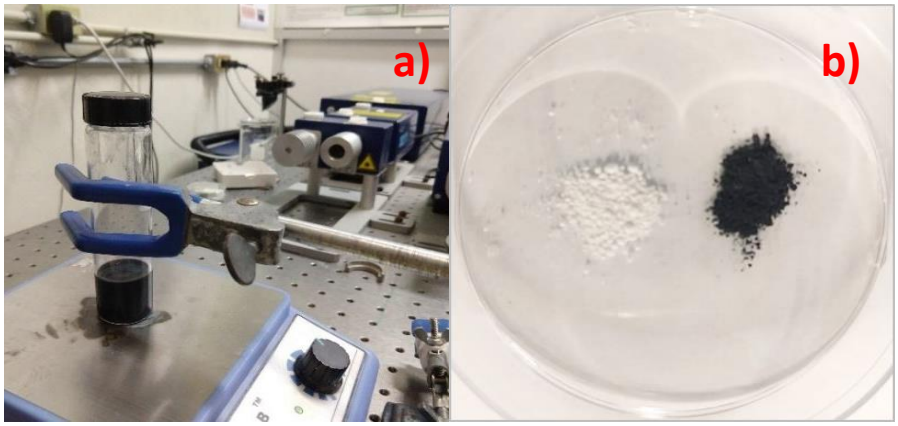

Figure 3. 1. Samples of synthetized black TiO_2 by pulsed laser irradiation method, a) black TiO_2 after laser irradiation, b) black TiO_2 powders after drying.

The drying process was carried out at room temperature in a petri dish, the average time for complete drying was 2 days. The sample was collected as powder as shown in figure 3.1 (b), where white TiO_2 powder is compared to black TiO_2 at 60 minutes of irradiation.

The nanopowders for each sample synthesized in water media are shown in the figure 3.2 (a). It can be observed an increasing darker black color by increasing irradiation time, the sample are labeled as B-TiO_2 X minutes (X= 45, 60, 75, and 90 minutes). The nanopowders for those samples were resulted in a fine powder in comparation of white TiO_2 powder, and the presence of sparkly particle was observed for the 60-, 75- and 90-minutes samples.

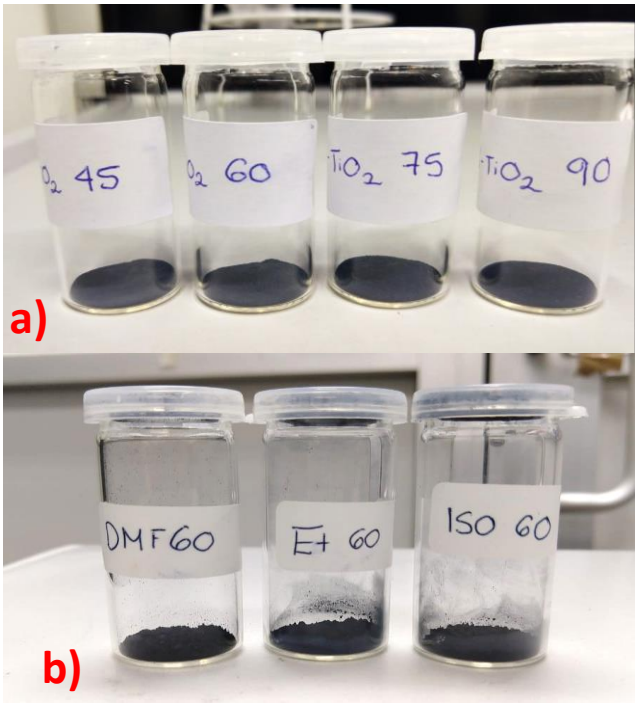

Figure 3. 2. Images of black TiO_2 nanopowders, (a) samples of black TiO_2 synthetized in water during 45, 60, 75, 90 minutes of laser irradiation, (b) samples of black TiO_2 synthetized in dimethylformamide (DMF), ethanol, and isopropyl alcohol by 60 minutes of laser irradiation

The same procedure was used to synthesize black TiO_2 in isopropyl alcohol, ethanol, and dimethylformamide (DMF) media. The irradiation time was set fixed at 60 minutes for these solvents. For those samples a darker black color was observed in comparison to the 60-minutes-water sample; ethanol, isopropyl alcohol and DMF in this order. In addition, the temperature in those samples was higher. The DMF sample was the thickest solution and for this sample it was necessary to use a low temperature oven to fast drying (150 ºC for 20 minutes) because its drying was supposed to be into 4 or 5 days. And for ethanol, isopropyl alcohol to obtain a completed drying, the oven was set at 100 ºC for 20 minutes as well. The final samples are shown in the Fig 3.2 (b), and respectively labeled as DMF 60, ET 60, ISO 60. In contrast to the

samples prepared in water, no sparkly particles were observed in the organic solvent samples but an adhering property to the surface for the ethanol and isopropyl alcohol was observed as in the Figure 3.2 (b).

The laser parameter applied for the synthesis were: wavelength of 532 nm, pulse duration of 10 ns and a frequency of 10 Hz. The energy was around 350 mJ/pulse which resulted in a fluence of 0.65 J/cm^2. The laser spot around 1 cm was ideal to irradiate more quantity of solution, meanwhile the interval between each pulse duration allowed to dissipate the proper heat transfer to obtain a like heating/melting process.

3.2 Characterization of modified black TiO_2

3.2.1 Crystal Structure

3.2.1.1 X-Ray Diffraction analysis

The results of the X-ray diffraction analyses of the black TiO_2 nanomaterials synthesized in liquid media are shown in Figure 3.3. The mainly identified phases are marked by A for anatase phase (PDF No. 04-007-0701) and R for rutile phase (PDF No. 04-008-7645). As indicated the figure 3.3, the main peaks and representative peaks for those samples are located at 2θ = 25.25º and 27.3º (for anatase and rutile respectively).

The initial X-ray diffraction patterns, namely white TiO_2 is observed to have a bigger peak in anatase phase and for the rest of the irradiate samples, the main peak of anatase was degreasing by irradiation time, at 45 minutes the dominate peak still was anatase, but at 60 minutes of irradiation, the main peak of rutile phase increased and anatase peak started to decrease; 75 and 90 minutes. The last sample, indicated as 90 min, has the bigger peak of rutile phase and the lower anatase peak

corresponded to the main peaks of the samples. This analysis is supported by the application of Rietveld method.

The Rietveld method is used to refinement of experiment data to obtain an optimal fit between experimental data and theoretical models. The refinement consists on least squares and the assumption that the profiles are known and the model for the crystal structure is available, it is useful to determinate the lattice parameters and quantitative phase composition.

$$S_y = \sum_i w_i \left(y_{i(obs)} - y_{i(cal)}\right)^2 \qquad \textit{Eq. 3.1}$$

The weight fraction (W_i) indicates the relative and absolute quantity of the phases present and it was calculated for anatase and rutile phase by the next mathematical:

$$W_a = \frac{S_a\,(ZMV)_a}{\sum_i S_i\,(ZMV)_i} \qquad \textit{Eq. 3.2}$$

Where *i* is the value of the *a* for a particular phase among the N phases present, S_a is the refined scale factor, Z is the number of the formula unites per unit cell, M is the molecular weight, and V is the unit cell volume. To know the efficiency of the model fit, it means, Goodness of fit (χ^2), equation 3.5, and R weighted profile (R_{wp}), values were evaluated to ensure fit (equation 3.3 and equation 3.4). The peak profiles were fitted with the pseudo-Voigt function.

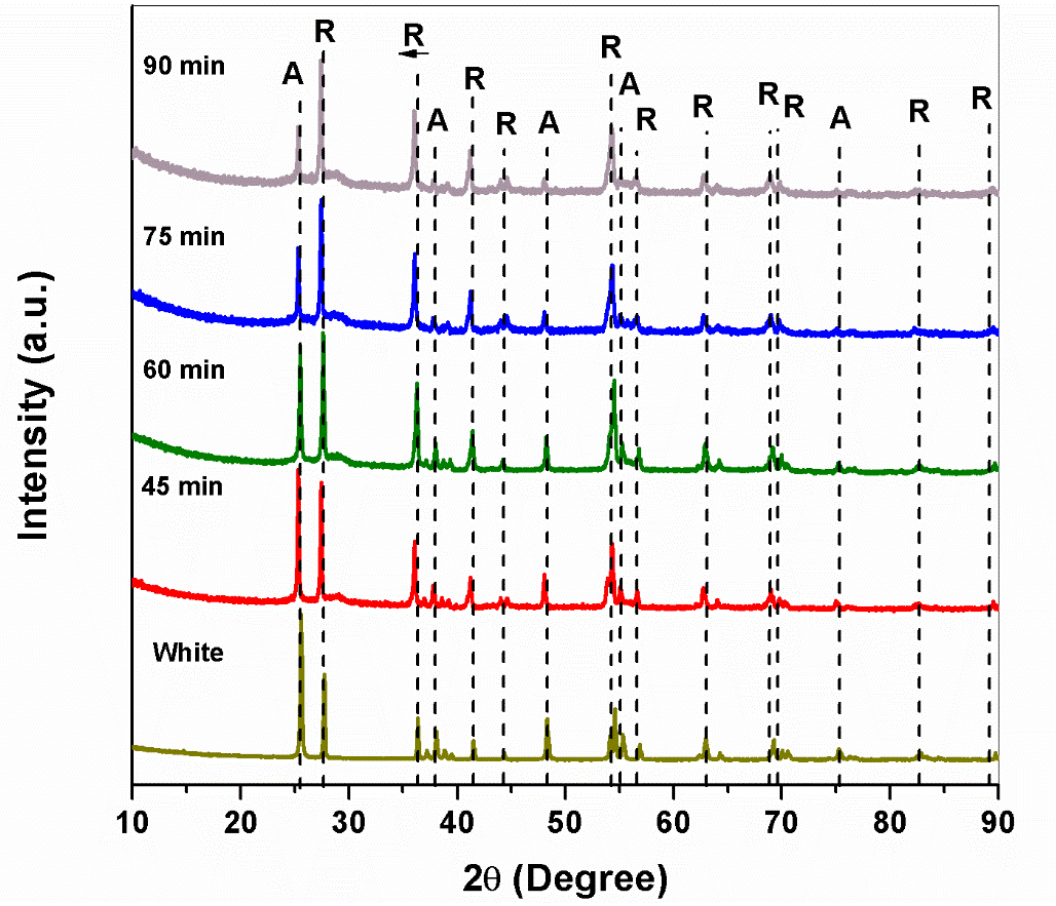

Figure 3. 3. Image of X-ray diffraction (XRD) patterns of white TiO_2 and irradiated samples by 45, 60, 75 and 90 minutes in water. The crystal structures of each samples are indicated as A=Anatase and R=Rutile.

$$R_e = \left[\frac{(N-M)}{\sum_i w_i (y_{i(obs)})^2}\right]^{1/2} \qquad \textit{Eq. 3.3}$$

$$R_{WP} = \left[\frac{\sum_i w_i (y_{i(obs)} - y_{i(cal)})^2}{\sum_i w_i (y_{i(obs)})^2}\right]^{1/2} \qquad \textit{Eq. 3.4}$$

$$\chi = \frac{R_{WP}}{R_e} = \left[\frac{\sum_i w_i (y_{i(obs)} - y_{i(cal)})^2}{N-M}\right]^{1/2} \qquad \textit{Eq. 3.5}$$

The results are listed in the table 3.1, which support the fact of the increasement of rutile phase and decrement of anatase phase quantity

related to the increment of irradiation time. Lattice parameter are also reported in the table 3.1 which are consistent to the theory.

Table 3. 1 Lattice parameters of black TiO_2 samples and calculated weighted profile value (Wt%).

Sample	Phase	Lattice parameters				Wt%
		a	b	c	α=β=γ	
White TiO_2	Rutile	4.592	4.592	2.957	90	41.8
	Anatase	3.783	3.783	9.512	90	58.2
45 min	Rutile	4.594	4.594	2.959	90	57.3
	Anatase	3.782	3.782	9.512	90	42.7
60 min	Rutile	4.595	4.595	2.959	90	63.96
	Anatase	3.781	3.781	9.509	90	36.04
75 min	Rutile	4.597	4.597	2.959	90	74.45
	Anatase	3.782	3.782	9.510	90	25.55
90 min	Rutile	4.600	4.600	2.960	90	72.89
	Anatase	3.783	3.783	9.513	90	27.11

Finally, the XRD patterns for the black TiO_2 synthesized in DMF, ethanol and isopropyl alcohol media are compared to black TiO_2 at 60 minutes in water and the white TiO_2 samples. The anatase patterns (PDF No.03-065-5714, PDF No. 01-083-2243 and PDF No. 01-071-1167) and rutile phase (PDF No. 01-079-6031, PDF No. 01-078-4185 and PDF No. 01-078-4189) are shown in Figure 3.4. In contrast to the samples in water media, the peak widening is more evident, and some peaks could not be identified, thus Rietveld method could not apply.

However, in Figure 3.4 the peak widening observed in the spectra of the samples DMF 60, ET 60 and ISO 60 also indicate the formation of

rutile and some amorphous nanomaterials. In addition, the data were normalized and similar to the samples in water media, the rutile main peak (1 1 0) increases but anatase peak remained slightly bigger (1 0 1). The second main peak is observed at 36.33º which belongs to anatase phase and for the DMF 60, ET 60 and ISO 60 samples not only shifts to 36.05º (1 0 1) to rutile phase but also increases its intensity. It is indicated with an arrow; this fact supports the evidence of phase transformation between anatase to rutile phase. The rutile peak at 41.2º (1 1 1) was also remarkably increased as well as anatase peak at 54.9º.

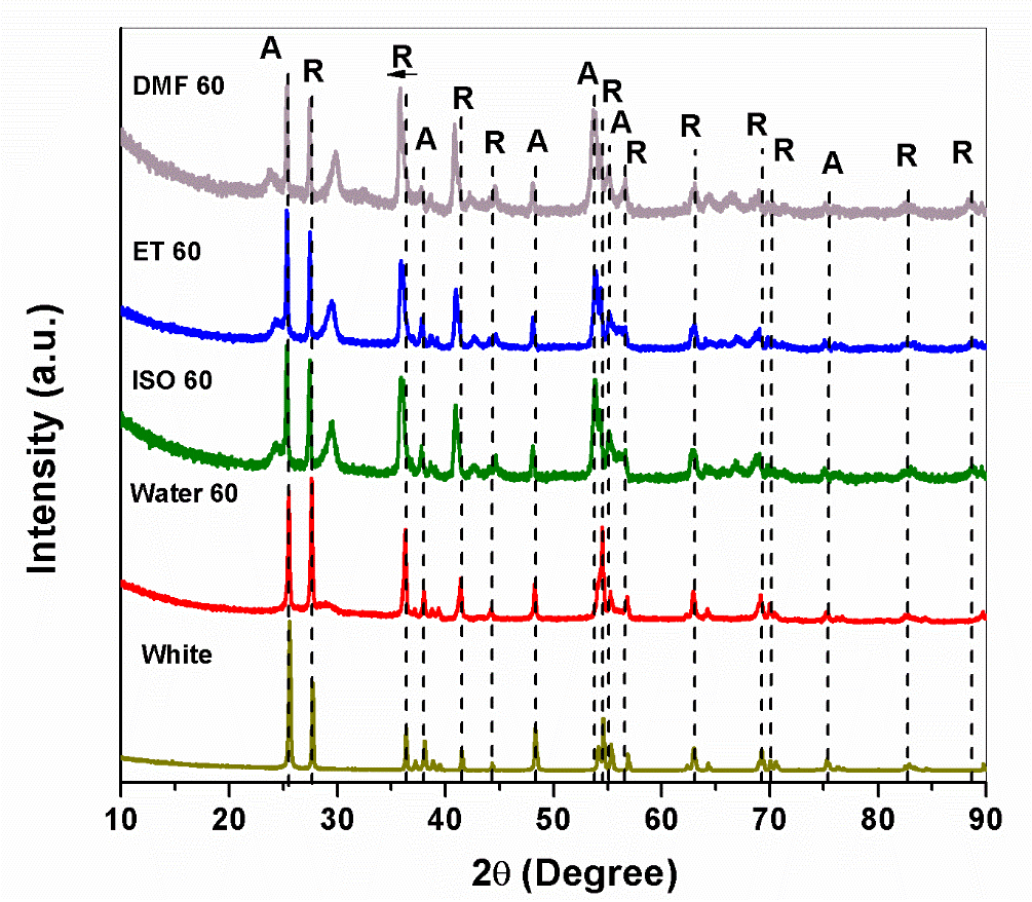

Figure 3. 4. Image of X-ray diffraction (XRD) patterns of white TiO_2, and irradiate d samples in DMF, ethanol, isopropyl alcohol and water media at 60 minutes. The crystal structures of each samples are indicated as A=Anatase and R=Rutile.

3.2.1.4 Raman analysis

The crystal structures were confirmed by Raman spectroscopy as well as the anatase-rutile transformation. In figure 3.5, Raman spectra of black TiO_2 synthesized in water and respective molecular vibrations from each peak for anatase and rutile phases are shown.

The vibrational frequencies of anatase peaks are known at 142, 162, 400, 517 and 641 cm^{-1} and for rutile 110, 234, 446, 612 and 737 cm^{-1}. For those samples, a widening in all peaks is observed after 45 minutes of irradiation. The main peak corresponds to anatase (143 cm^{-1}) and the second major peak is at 395 cm^{-1} also corresponds to anatase phase. A new peak at 428 cm^{-1} appeared after 45 minutes of irradiation and near to the rutile peak. The next peak at 516 cm^{-1} (anatase) disappeared after 75 minutes. The last peak corresponds to anatase at 635 cm^{-1} and it started to shift at 616 cm^{-1} (rutile peak).

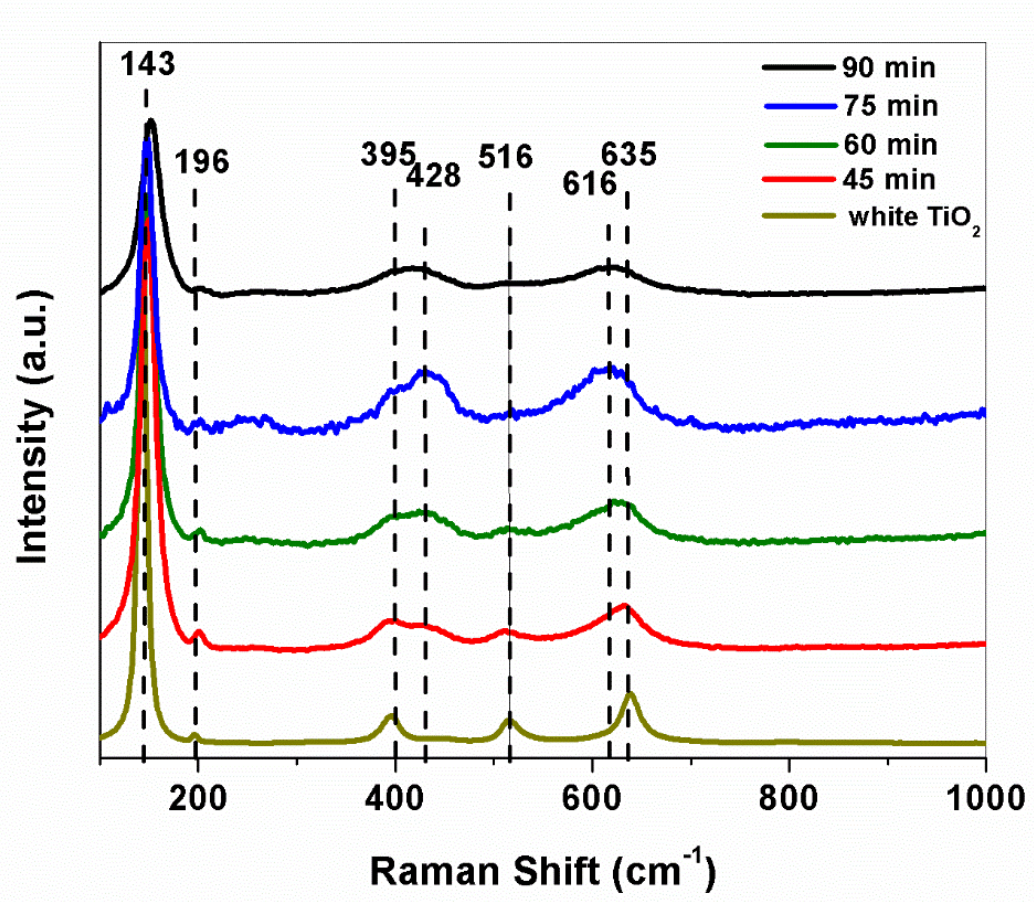

Figure 3. 5. Raman spectra of white TiO_2 (yellow), and irradiated samples by 45 (red), 60 (green), 75 (blue) and 90 minutes (black) in water.

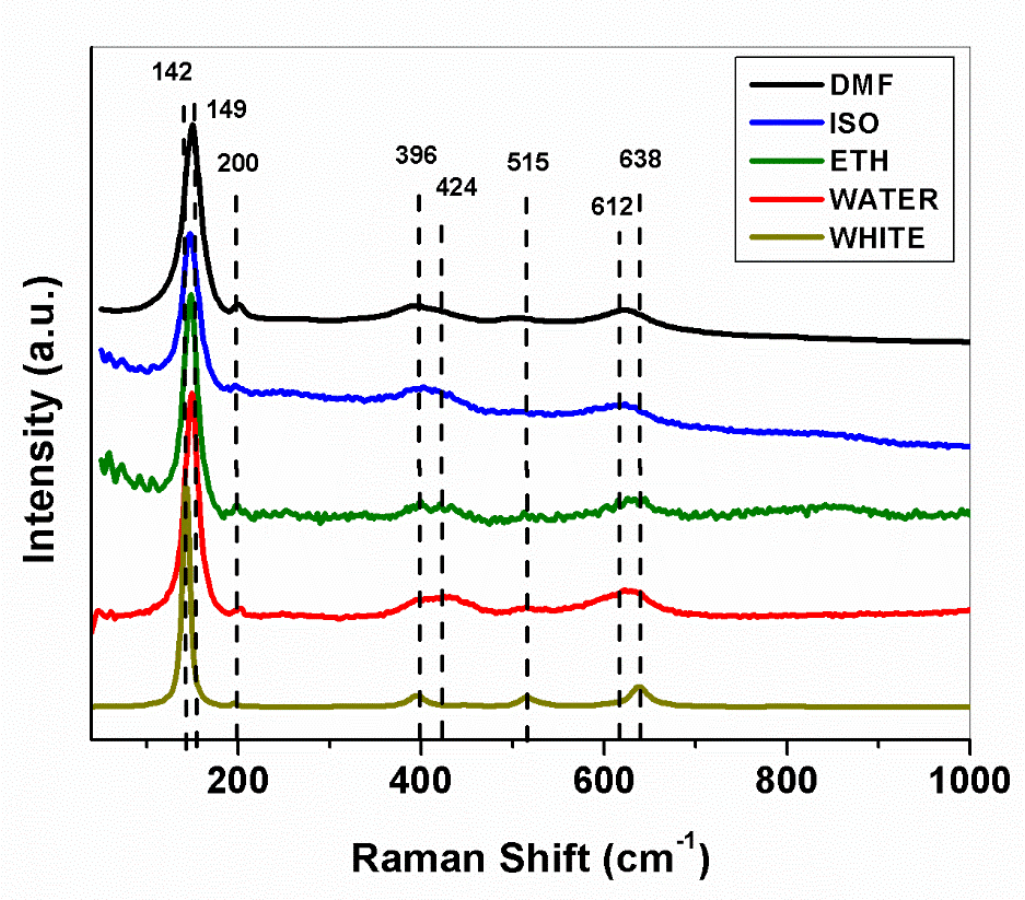

Figure 3. 6. Raman spectra of white TiO_2 (yellow), and irradiated samples by 60 minutes in water (red), ethanol (green), isopropyl alcohol (blue) and DMF (black).

The results for the black TiO_2 synthetized by DMF, isopropyl alcohol and ethanol are also compared to white TiO_2 and water at 60 minutes in Figure 3.6. Similarly, to the sample synthesized in water at 60 minutes, the samples DMF 60, ISO 60 and ET 60 present a widening in all peaks and the evidence of shifting at 396 and 638 cm^{-1} to 424 and 612 cm^{-1}. The table 3.2 resume those peaks in the table, as we can see the at 60 minutes in isopropyl alcohol and ethanol media the anatase pick disappear completely.

Table 3.2 Peaks of Raman spectra.

Raman Shift (cm^{-1})					
Sample	A	A	A	A	R
White TiO_2	142.55	196.5	396.15	515.7	638.2
Water 60	149.3	202.4	424.1	514.7	621
Ethanol 60	150.15	200.3	395.06	-	624.55
Isopropyl alcohol 60	147.26	197.4	401.811	-	612
DMF 60	148.22	198.4	399	513	614.91

3.2.2 Chemical state analysis

3.2.2.1 X-ray photoelectron spectroscopy (XPS)

The X-ray photoelectron spectroscopy (XPS) is a surface characterization technique which allows to identify the composition and chemical states of the elements present in the samples. It is possible to identify elemental composition of the surface by a low-resolution spectrum analysis known as survey spectrum. The chemical states are evaluated by the chemical shifts in elemental binding energy by high resolution photoelectron spectra analysis. Depending on the chemical states and modification in material, the energy of the binding energy changes and can be observed in the core level photoemission peaks.

Figure 3.7 shows a high-resolution scan of Ti 2p for white TiO_2, where its binding energies of $2p_{3/2}$ and $2p_{1/2}$ are 458.33 eV and 464.28 respectively, thus spin-orbit split is 5.95 eV, which matches with the reported split for TiO_2. On the other hand, the irradiated samples at 45, 60 and 75 minutes, there is a slight shift in energy in comparation of 90

minutes- sample where is 0.5 eV a shift in B.E. The phase transition of anatase to rutile produce oxygen vacancies, consequently, a shift in the binding energy of oxygen agrees to the O1s scan analysis shown in Figure 3.8, where it is observed a shift in B.E. from 529.52 eV of the white TiO_2 (as the reported value) to 530.23 eV for 90 minutes of irradiated black TiO_2.

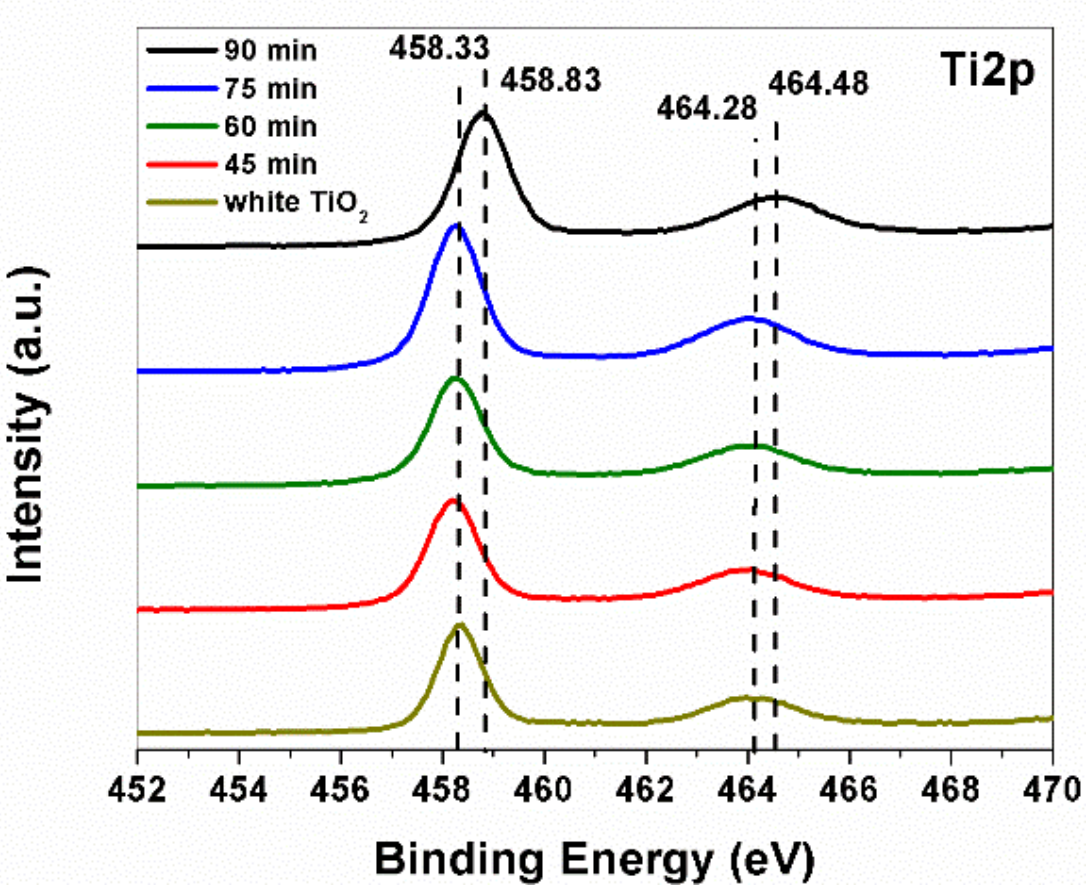

Figure 3. 7. XPS high resolution spectra of Ti 2p for white TiO_2 and irradiated samples by 45 minutes (red), 60 minutes (green), 75 minutes (blue) and 90 minutes (black) in water.

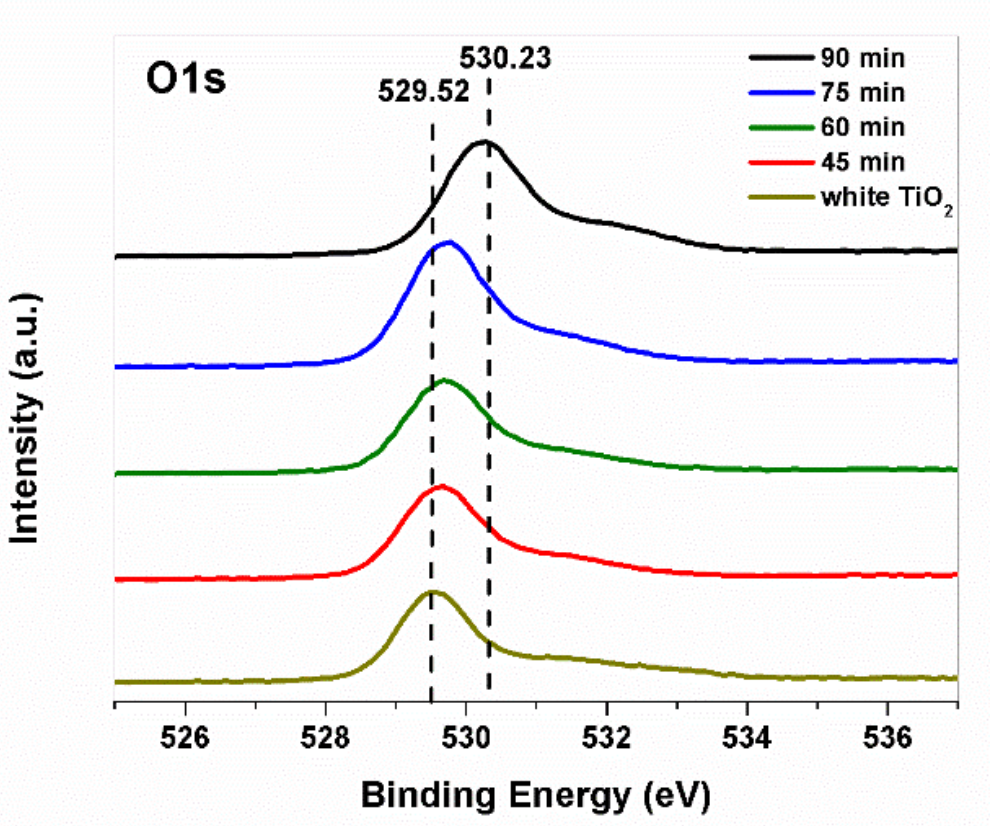

Figure 3. 8. XPS high resolution spectra of O1s for white TiO_2 and irradiated samples by 45 minutes (red), 60 minutes (green), 75 minutes (blue) and 90 minutes (black) in water.

The first set of analysis provided an overview of the relationship in binding energies and general effects due to the irradiation time in samples. Changes in binding energies were properly compared using differentiation in energy (dC/dE), where difference in shift point (maximum and minimum), width, and intensity of the peaks can be well compared. The Figure 3.9 (water) in the same way differentiation in binding energy increases by increase in time of irradiation, although in Figure 3.8 sample of 90 min seems to be higher due to the shift energy but intensity and width in 75 min peak contribute more to the differential energy, figure 3.10.

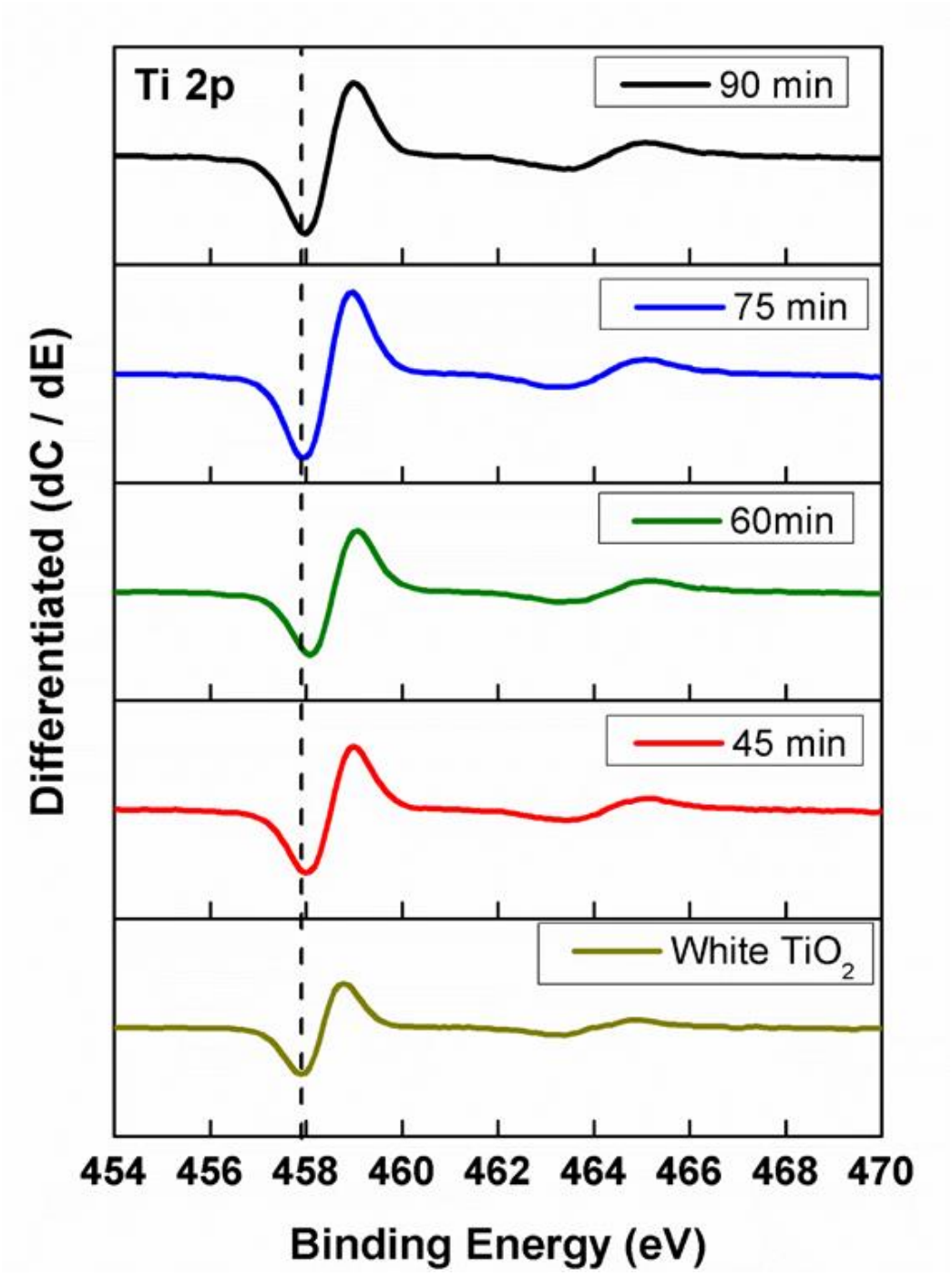

Figure 3. 9. Images of derivates of XPS high resolution spectra of Ti 2p for the synthesized black TiO_2 in water.

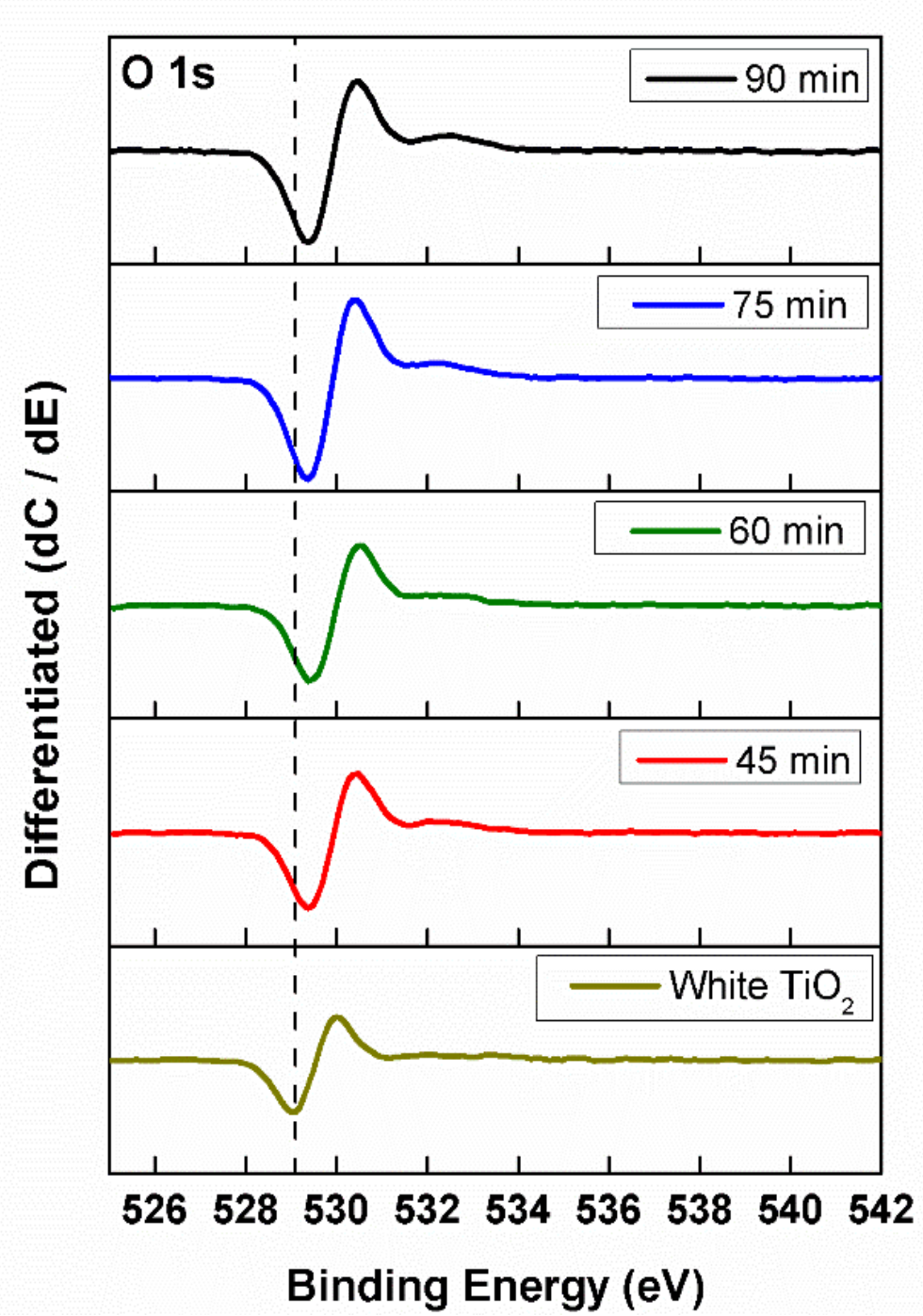

Figure 3. 10 Images of derivates of XPS high resolution spectra of O1s for the synthesized black TiO_2 in water.

The same analysis was applied to the samples of black TiO_2 synthesized in DMF, Ethanol, isopropyl alcohol and they were also compared with white and water at 60 minutes of irradiation. High

resolution scan of Ti 2p is shown in Figure 3.11, the binding energies for the samples are 458.33 eV for white TiO_2, 458.54 eV for Water 60, 458.72 eV for ET, 458.69 eV for ISO and 458.7 eV for DMF.

In the same way, the binding energies from high resolution of O1s were compared for the samples and are shown in Figure 12. For white TiO_2 a single peak at 529.55 eV was detected, contrary to the rest of the samples where 2 peaks were identified. The corresponded peaks of Water 60 sample were 530.1 eV and 539.97 eV, where the first peak suggest an extra peak at 532.2. Next samples presented two peaks which correspond to 458.72 eV and 540.17 for ET 60 and 458.69 eV and 540.1 for ISO 60 and 458.7 eV and 540.19 for DMF 60 sample.

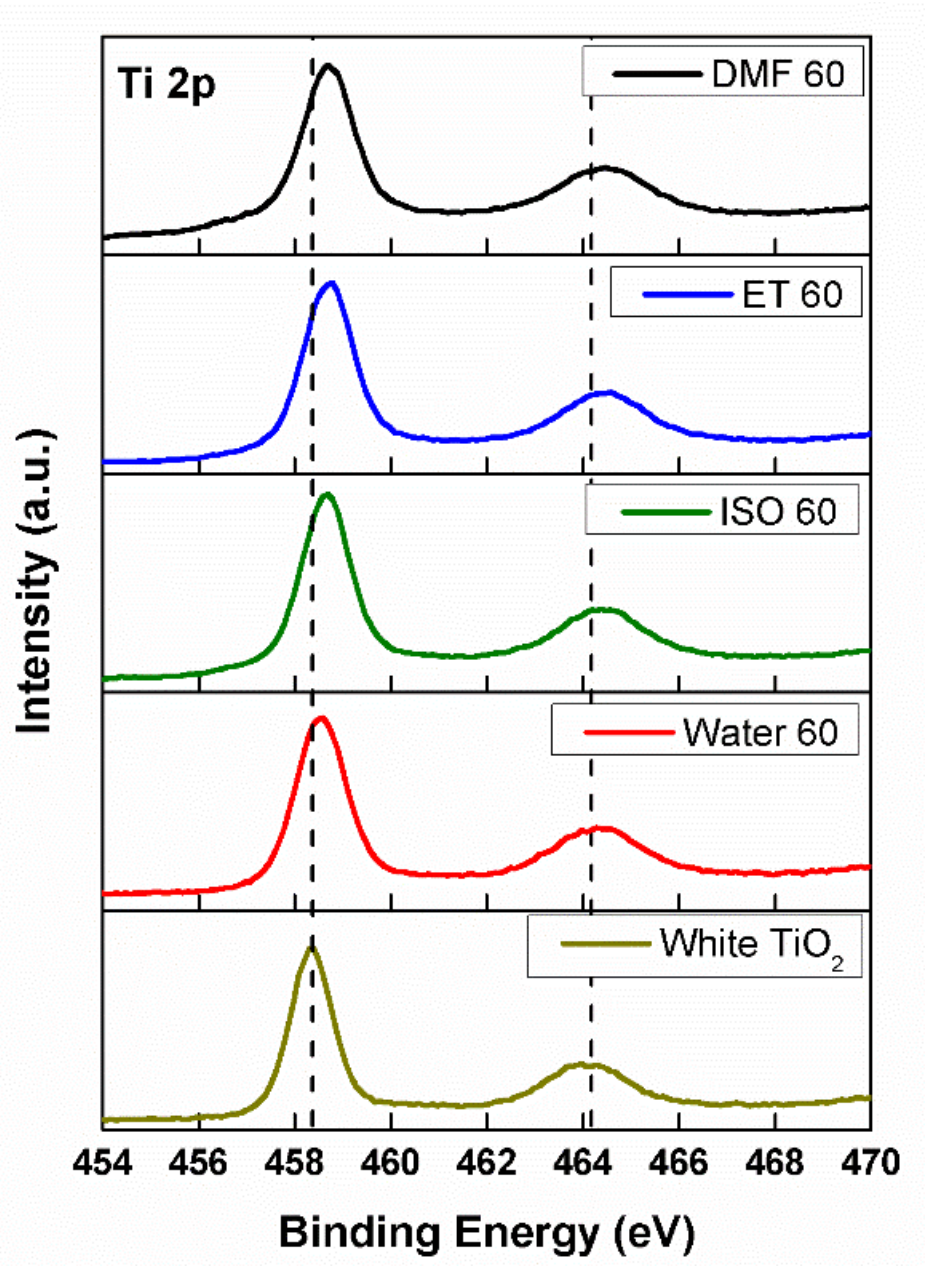

Figure 3. 11 XPS high resolution spectra of Ti 2p for white TiO_2 and irradiated samples at 60 minutes in DMF, ethanol, isopropyl alcohol, and water.

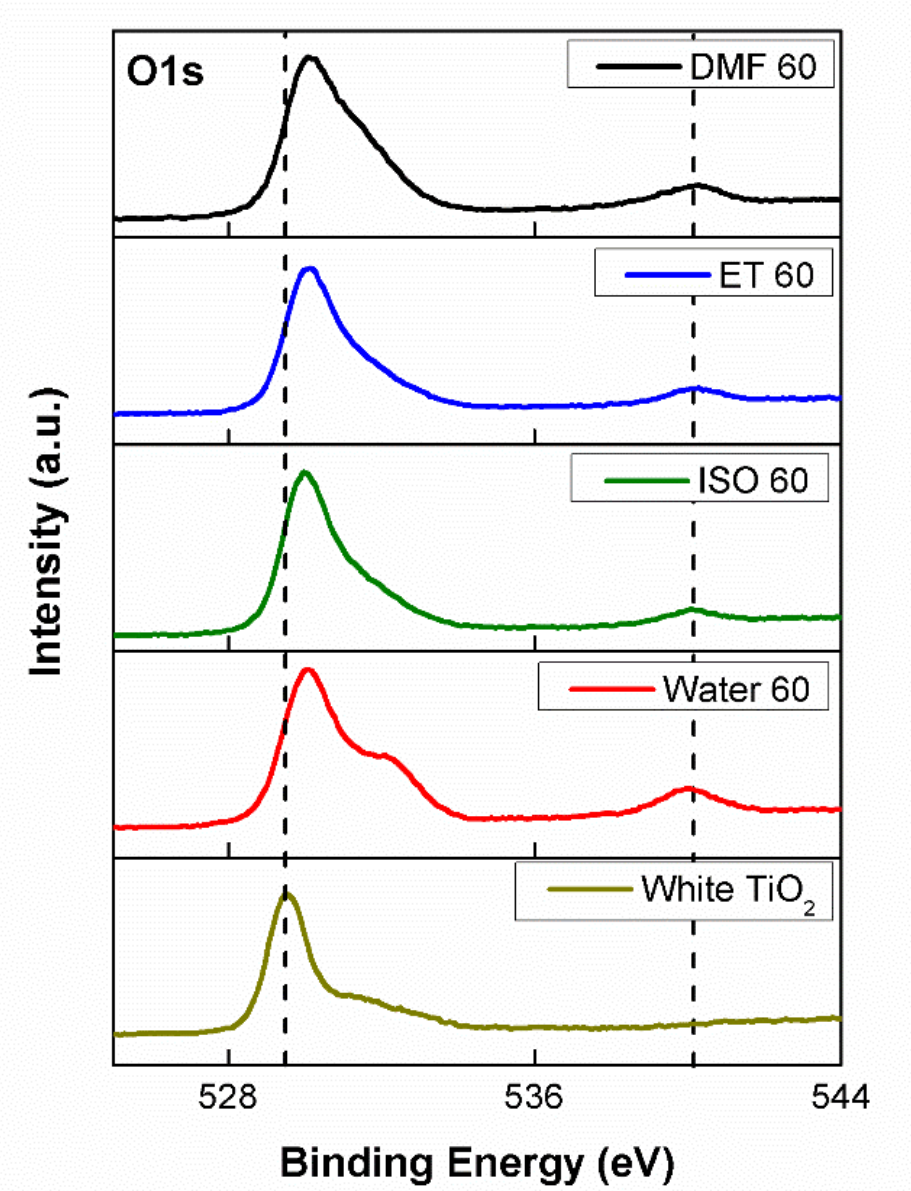

Figure 3. 12. Images of XPS high resolution spectra of O1s for white TiO_2 and irradiated samples at 60 minutes in DMF, ethanol, isopropyl alcohol, and water.

Furthermore, those samples were also compared by differentiation in energy (dC/dE). Figure 3.13 compares Ti 2p differentiation, change in binding energy for ethanol 60 sample is slightly higher as DMF 60 sample. The results for ethanol and isopropyl are like water media results. Subsequently, the Figure 3.14 confirms the binding energy shift for O1s in organic media samples. According to Figure 3.12 and 3.14, the

widening is caused due to the nature of C-O groups derivate by the organic solutions present during the synthesis.

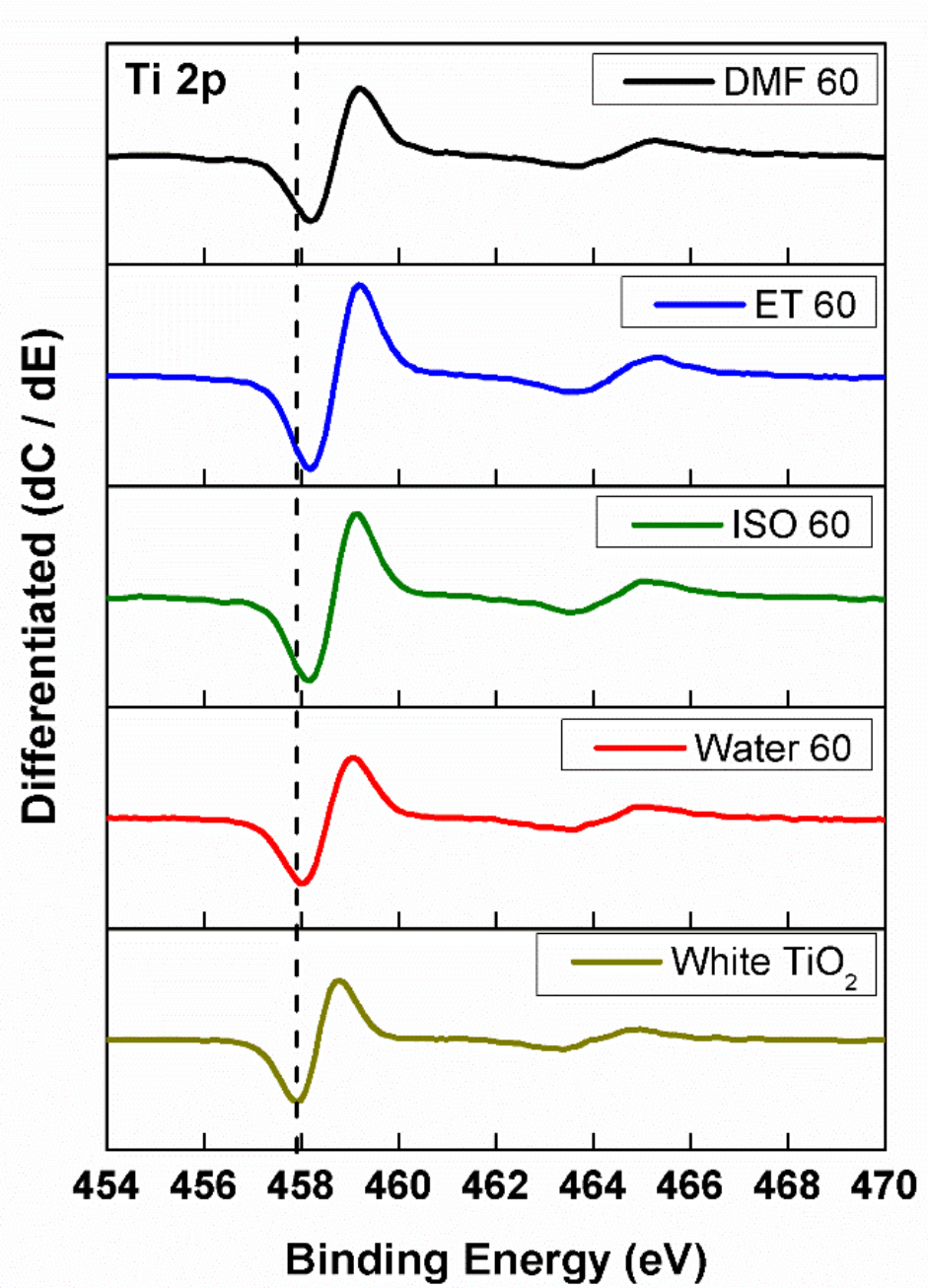

Figure 3. 13. Images of derivates of XPS high resolution spectra of Ti2p for white TiO_2 and irradiated samples at 60 minutes in DMF, ethanol, isopropyl alcohol, and water.

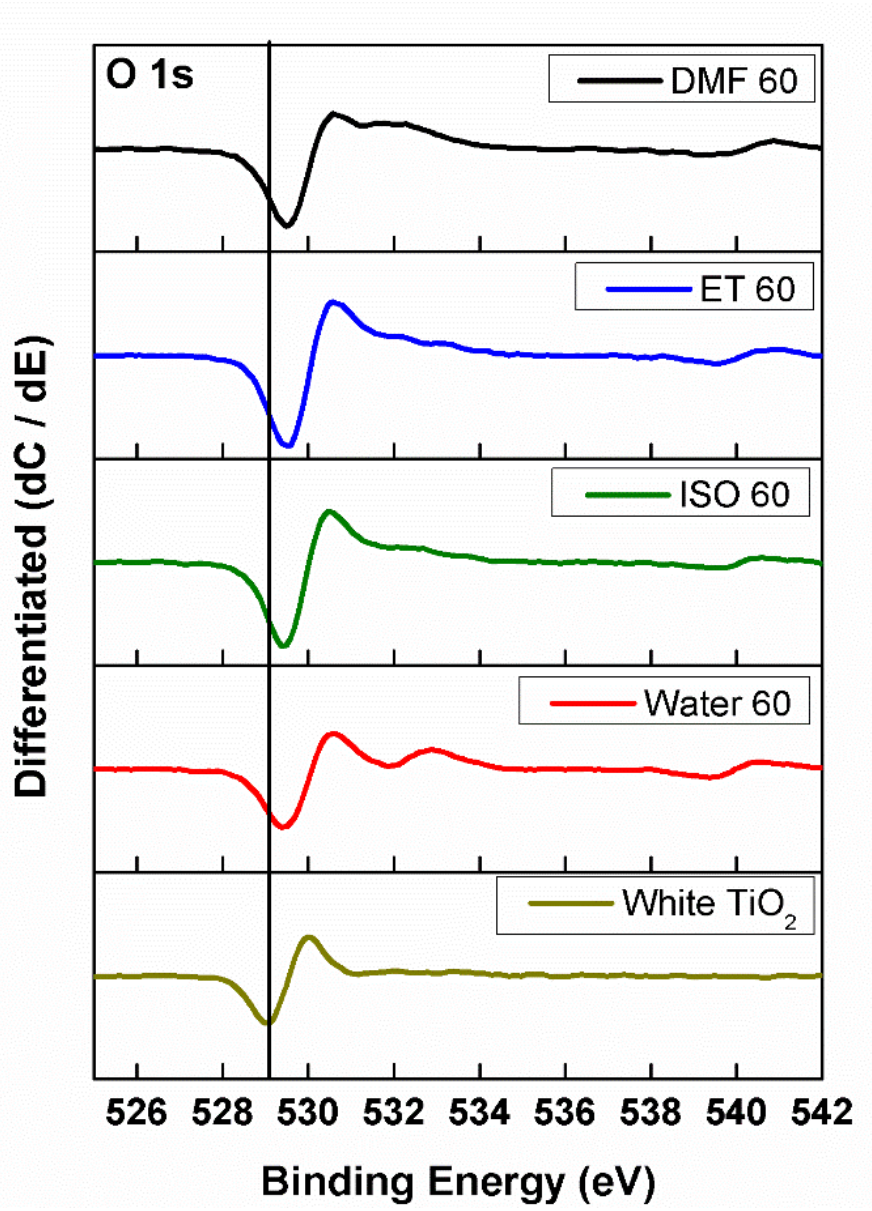

Figure 3. 14. Images of derivates of XP high resolution spectra of Ti2p for white TiO_2 and irradiated samples at 60 minutes in DMF, ethanol, isopropyl alcohol, and water.

In summary, the laser irradiation in liquid media produces changes in chemicals states due to defects incorporation caused by the interaction laser-material. The shift and widening produced in samples clearly increased with time of irradiation, also by change of liquid media.

3.2.2.3 Valence band analysis

The valence band of TiO_2 consists of electrons from Ti 3d level and an overlapping orbitals of O 2p level [2]. Valance band analysis was used to analyzes the change in valence band edge, which is expected to widen, thus the narrowing in band gap can be achieved. Nevertheless, some molecular orbitals possess a high degree of hybridization and photoelectron signal shows subtle and varied shift in peaks, thus those spectra are not useful for quantification analysis, but it can be useful to compare samples with a reference material.

The first results correspond to irradiated samples in water media for 45, 60, 75 and 90 minutes as shown in Figure 3.15. Those results demonstrated a subtle change in valence band energy. The straight-line part observed in every spectrum was extrapolated to the axis as shown in the figures 3.15 and 3.16. The reference spectrum according to white TiO_2 correspond a binding energy at 2.24 eV. Subsequently, 2.33 eV for 45 min, 2.52 eV for 60 min, 2.40 eV for 75 min and 2.35 eV for 90 min sample. In addition, the valence band spectrum in white TiO_2 seems to exhibit 2 wide peak and for the rest of the spectra seem to two peaks reach the same level and result in consolidation of one wide peak.

The incorporation of carbon introduced new states C 2p near to the VB edge to narrow the band gap of TiO_2 [31]. This fact can explain the growing of the second like-peak observed in the valence spectra of DMF 60, ISO 60 and ET 60 samples (Figure 3.16). The corresponding binging energies for those samples are the follows, 2.52 eV for water 60, 2.53 eV for ET 60, 2.49 eV for ISO 60 and 2.12 eV for DMF 60.

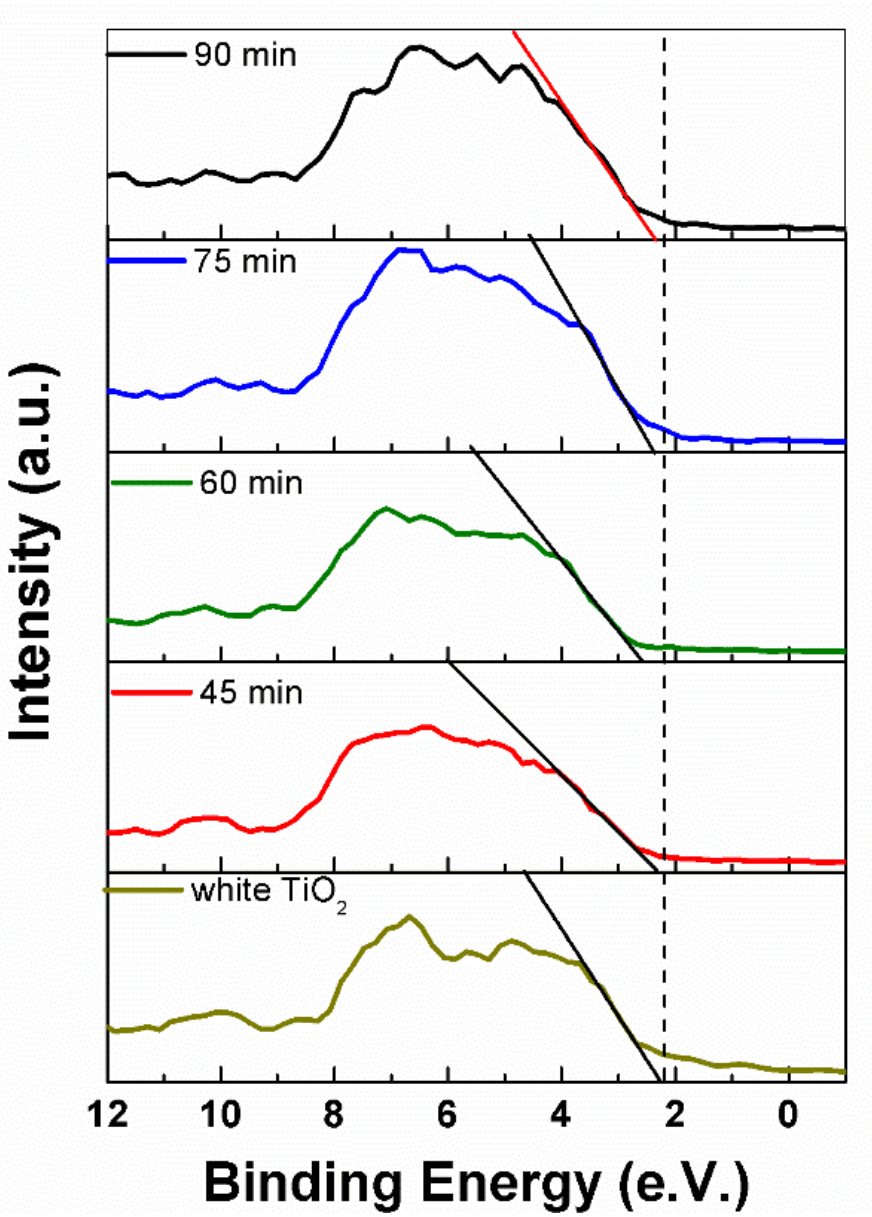

Figure 3. 15. Valence band spectra of white TiO_2 and irradiated samples by 45, 60, 75 and 90 minutes in water.

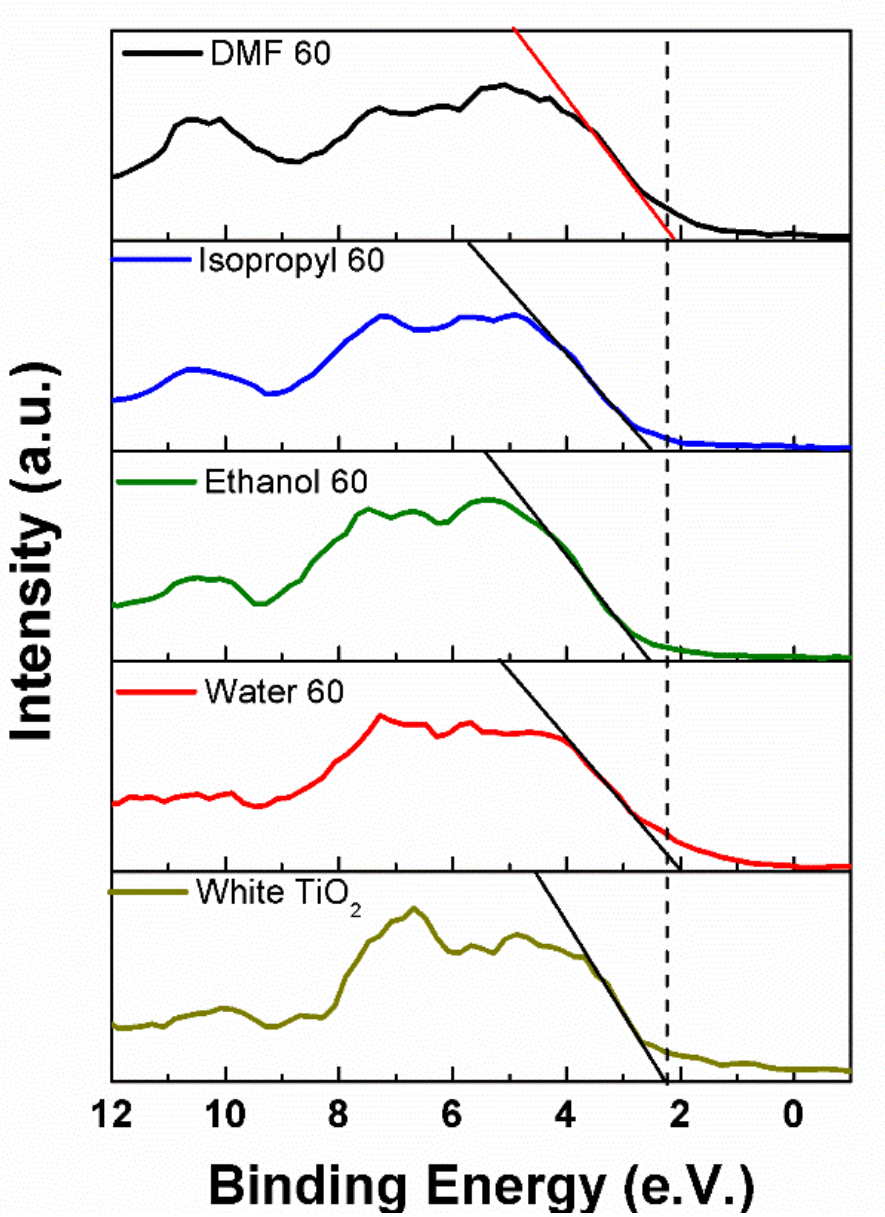

Figure 3. 16. Valence band spectra of white TiO_2 and black TiO_2 synthetized in DMF, Ethanol and Isopropyl alcohol for 60 minutes of laser irradiation

3.2.2.4 Chemical states mapping

The chemical state mapping was analyzed for water 60, DMF 60, ISO 60, and ET 60 samples. The scan area was 1 mm x 2 mm, using 2 scan 20.1 s and 0.10 eV. Figure 3.17 shown scans of Ti at 448.05 eV (blue) and O1s at 525.08 eV (red) of electron binding for water 60, ethanol

60, isopropyl 60 and DMF 60. The white color indicates low concertation of the analyzed element and darker color indicate high concentration.

Scans of water 60 sample revels high concentration of Ti and O coincide, and the element distribution is not uniform and Figure 3.18 (a). On the contrary, Ethanol 60 and Isopropyl 60 exhibit an enhanced element distribution but oxygen concentrations are higher as the water 60 sample. Figure 3.18 (b) shows the distribute coupling joint of Ti and O for ethanol 60 sample.

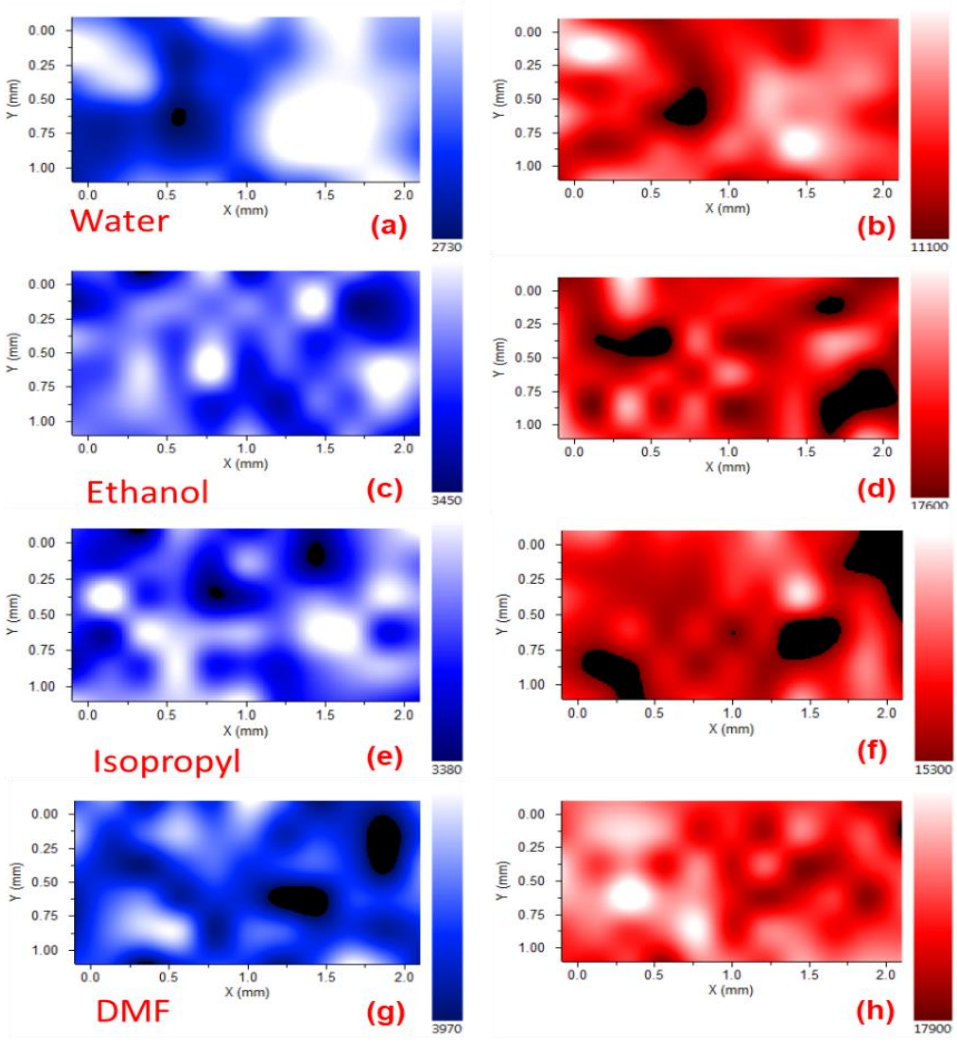

Figure 3. 17. Chemical state mapping for Water 60, Ethanol 60, Isopropyl 60 and DMF 60, (a) Ti2p scan of water 60, (b) O1s scan of water 60, (c) Ti2p scan of ethanol 60, (d) O1s scan of isopropyl 60, (e) Ti2p scan of Isopropyl 60, b) O1s scan of isopropyl 60, , (e) Ti2p scan of DMF 60, b) O1s scan of DMF 60.

Similarly, Isopropyl 60 sample exhibit an enhance distribution, but an agglomerate oxygen concentration is also observed. At last, Figure 3.17 (g) and (h), shows a proper element distribution and as well. Figure 3.18 (d) confirms the distributed concentration of oxygen but the lower oxygen concentration, figure 3.17 (h), in comparation of Water 60 (figure 3.17 (b)), ethanol 60 (figure 3.17 (d)), and Isopropyl 60 (figure 3.17 (f)). This statement is consistent with the percent composition of oxygen in the liquid medias, 88% O in water, 34% O in ethanol, 26% O in isopropyl alcohol and 21% O in DMF.

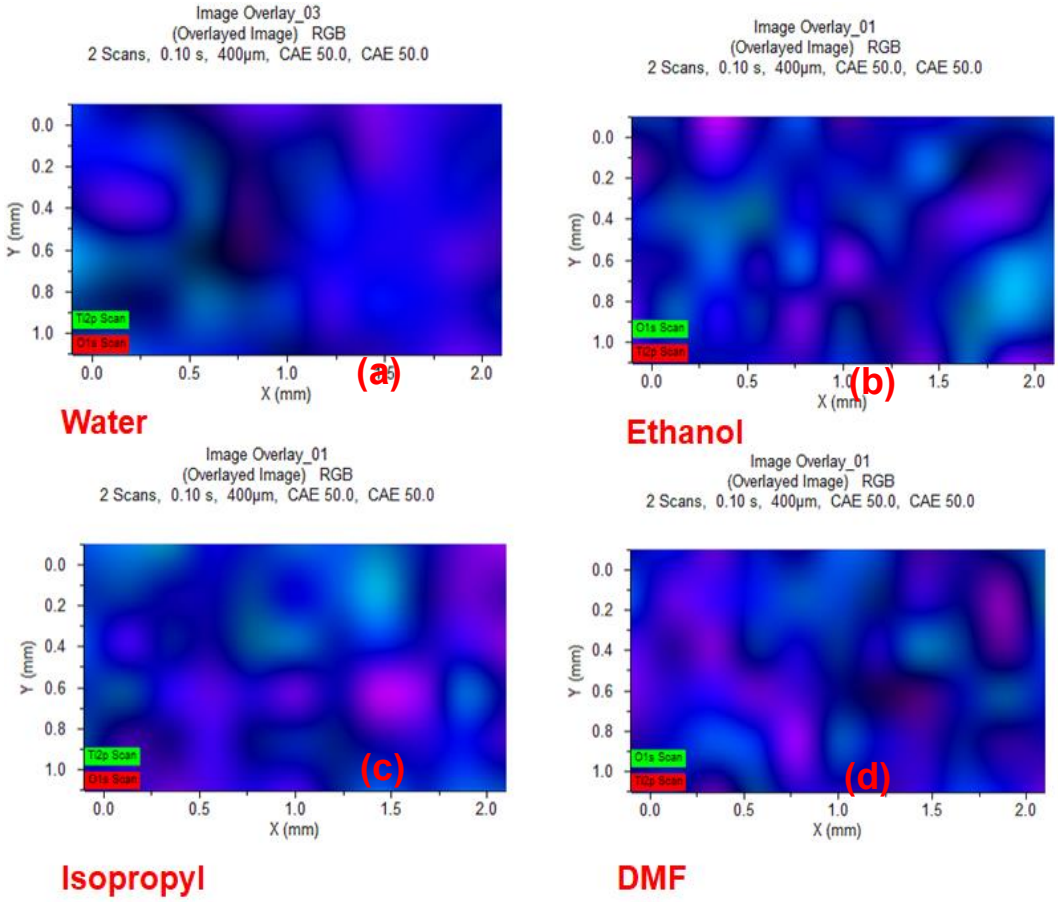

Figure 3. 18. Chemical state mapping images of Ti 2p (blue) and O1s (purple) of white TiO_2 and black TiO_2 synthetized in DMF, Ethanol and Isopropyl alcohol for 60 minutes of laser irradiation.

3.2.3 Morphology and particle size

Modification in morphology of irradiated particle were studied by scanning electron microscopy (SEM) technique, which provides micrographs at different magnifications to examine particle size as well. The present section examines the effect of laser irradiation in the morphology and the relationship between liquid media and particle size of the nanomaterials.

3.2.3.1 SEM analysis

Figure 3.19 presents the SEM images in different scale bars (5, 2, 1 μm and 500 nm) of white TiO_2 and irradiated samples at 45, 60, 75 and 90 minutes in water media. At first, white TiO_2 nanoparticles presented rectangular morphology with edges and corners, the size is also divers and agglomeration in particles is also observed. Changes in morphology are already presented at 45 minutes of irradiation, the micrography at 1 μm of 45 min sample still shows morphology of white TiO_2 nanoparticles and the next figure (500 nm) exhibit smaller particles produced by fragmentation of bigger particles. This effect is also reported in another articles after post irradiation.

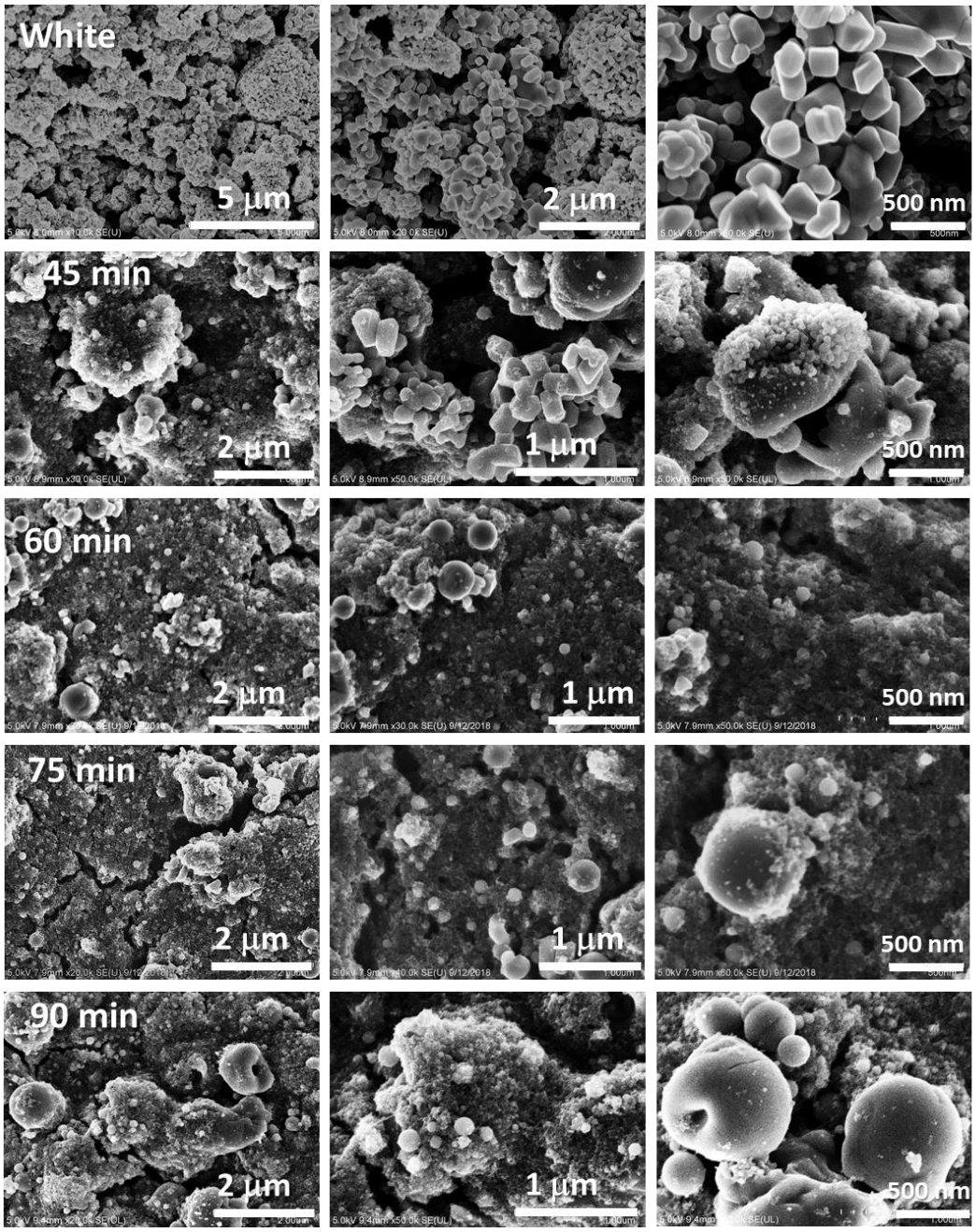

Figure 3. 19 SEM images of black TiO_2 synthetized in water media at 45, 60, 75 and 90 minutes.

Showing up next, 60 min sample (at 2 µm) exhibit agglomeration of big particles, in addition, amorphous bigger and spherical smaller particles are also observed (at 1 µm). Smaller particles are still summertide to laser irradiation the absorption of the radiation causes non-

linear like melting process. For the 75 min sample, the same effect under the nanoparticles is also observed, and in figure at 500 nm can be clearly observed agglomerations and fragmentation of the particles. Comparable, 90 min sample also presented the characteristics and morphology shows amorphous shapes in nanoparticles.

The identified effects due to laser irradiation can be explained by the energy absorption of the nanoparticles and the heating/melting effect as result. Previous studies showed anatase-rutile transformation and fragmentation phenomenon in post irradiation at 0.23 J/cm^2 of fluence [35]. The present results show those effects caused by laser irradiation at 0.65 J/cm^2 and confirms the like-melting effect and the anatase-rutile transformation observed in the XRD and Raman analysis results. The initial anatase nanoparticles with denser particle packing induce interface nucleation of anatase particles in contact at low temperatures to contribute to the rutile nucleation. On the other hand, lower particles packing suffer surface nucleation at intermediate temperatures meanwhile bulk material required high temperatures to the transformation [36]

Furthermore, the like-melting process promote the formation of bigger nanoparticles, those bigger particles can suffer laser fragmentation producing smaller nanoparticles, subsequently, smaller particles are heating and nuclei to form new nanoparticles. In the addition, amorphous morphology may be caused by the surface defects caused by the laser irradiation. As shown in Figure 3.20, DMF 60, ISO 60 and ET 60 (2 μm) exhibit agglomeration and micro size particles with spherical and amorphous shapes. However, smaller nanoparticles are observed at microscopies at 1 μm, those particles are also agglomerated around the biggest particles. In the same way, nanoparticles can be observed around the surface of the bigger particles, it can be better appreciated in the isopropyl 60 micrography at 500 nm. Those results confirmed the effects

caused by laser irradiation for both experiments. In summary, bigger particles are obtained by organic liquid media.

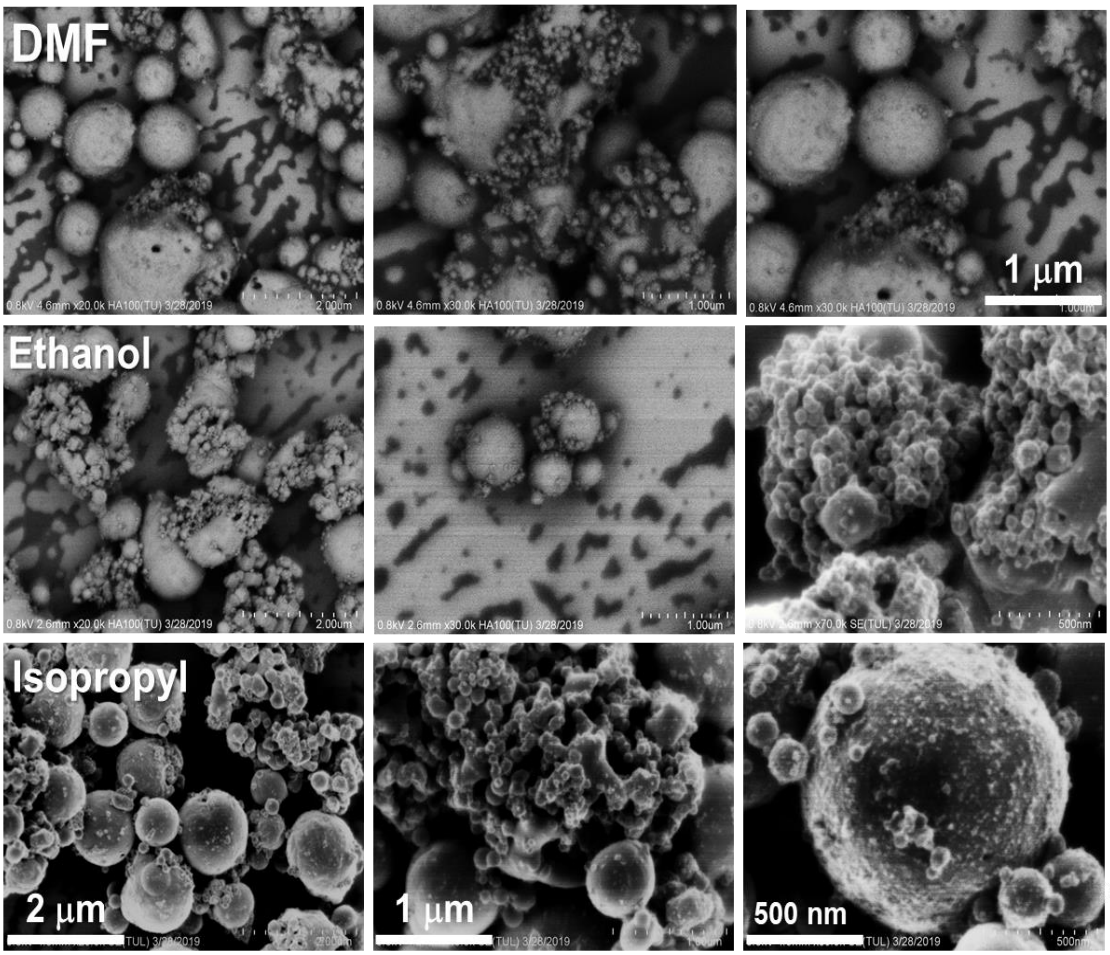

Figure 3. 20. SEM images of black TiO_2 synthetized in DMF, Ethanol and Isopropyl alcohol by 60 minutes of laser irradiation.

3.2.4 Optical properties

The optical properties were examined by UV-Visible diffuse reflectance spectra and then absorbance spectra for those samples were evaluated. Furthermore, the band gap for each sample were estimated by Kubelka-Munk function method. The results are explained in detail in the next section.

3.2.4.1 Diffused reflectance

The results for the diffused reflectance of the samples synthesized in water media are summarized in Figure 3.21. Significant positive correlation between diffuse reflectance and color change in the samples agree with electronic-optic properties change from the white TiO_2 nanomaterial.

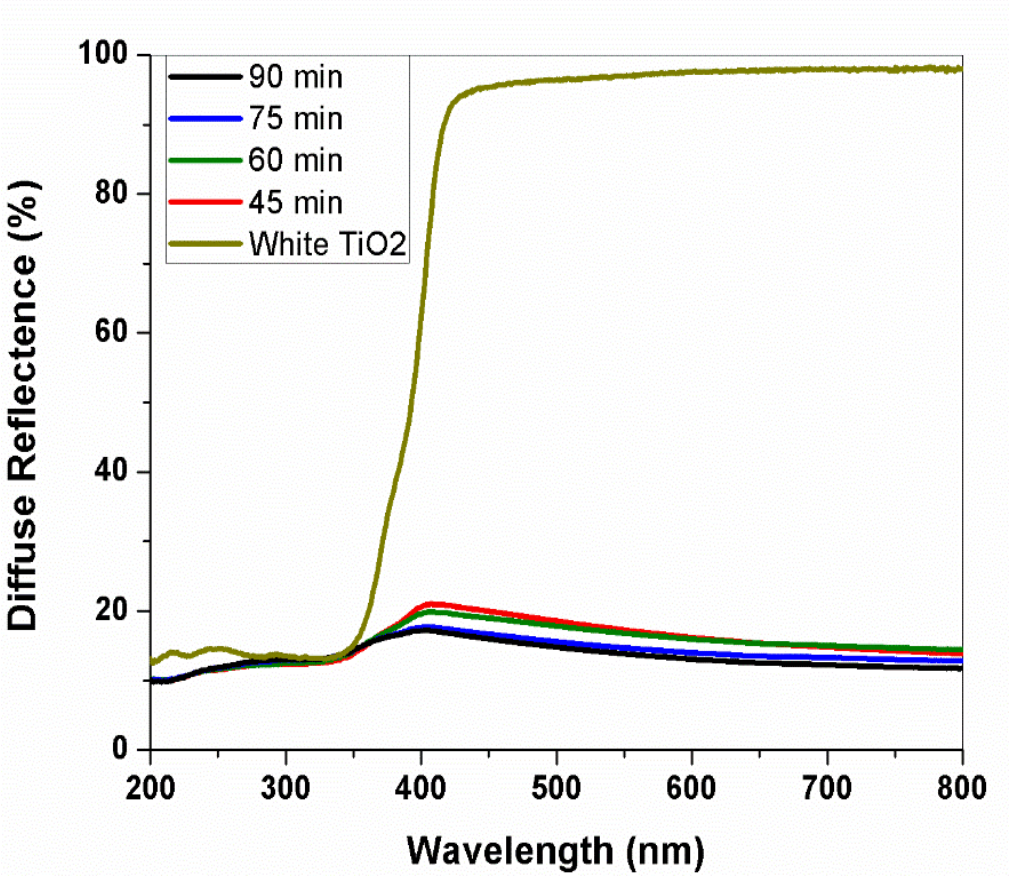

Figure 3. 21. Diffuse reflectance (%) spectra of b white TiO_2 and irradiated samples by 45, 60, 75 and 90 minutes in water.

3.2.4.2 Absorbance spectra analysis

The absorbance spectra were evaluated from diffuse reflectance results by the next equation,

$$A = \log\left(\frac{1}{R}\right) \qquad \textit{Eq. 3.6}$$

Where R is the diffuse reflectance value from Figure 3.21. The evaluated absorbance results from 45, 60, 75 and 90-min samples in

water media were plotted in Figure 3.22. From this Figure important information from this analysis is obtained to characterize the optical properties.

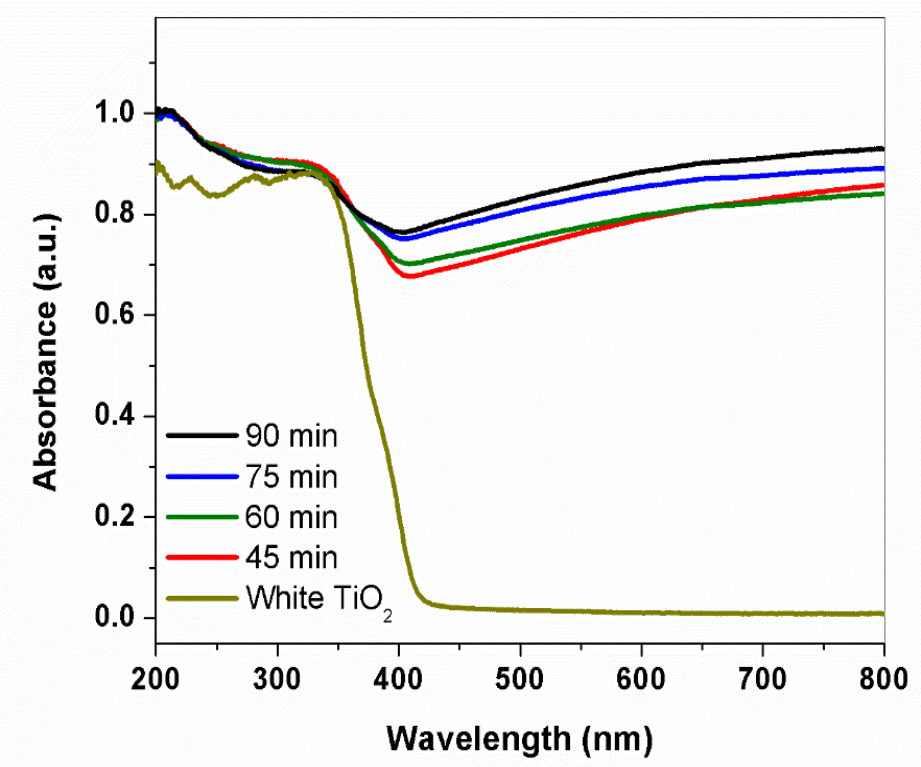

Figure 3. 22. Absorbance spectra of white TiO_2 and irradiated samples by 45, 60, 75 and 90 minutes in water.

Furthermore, DMF 60, ISO 60 and ET 60 samples were also analyzed in the same way. Figure 3.23 shows the comparation of water 60 sample vs organic solvents media. Those samples resulted in an enhance absorbance in visible region since carbon facilitate the absorption of visible light when carbonaceous species are at the surface [31].

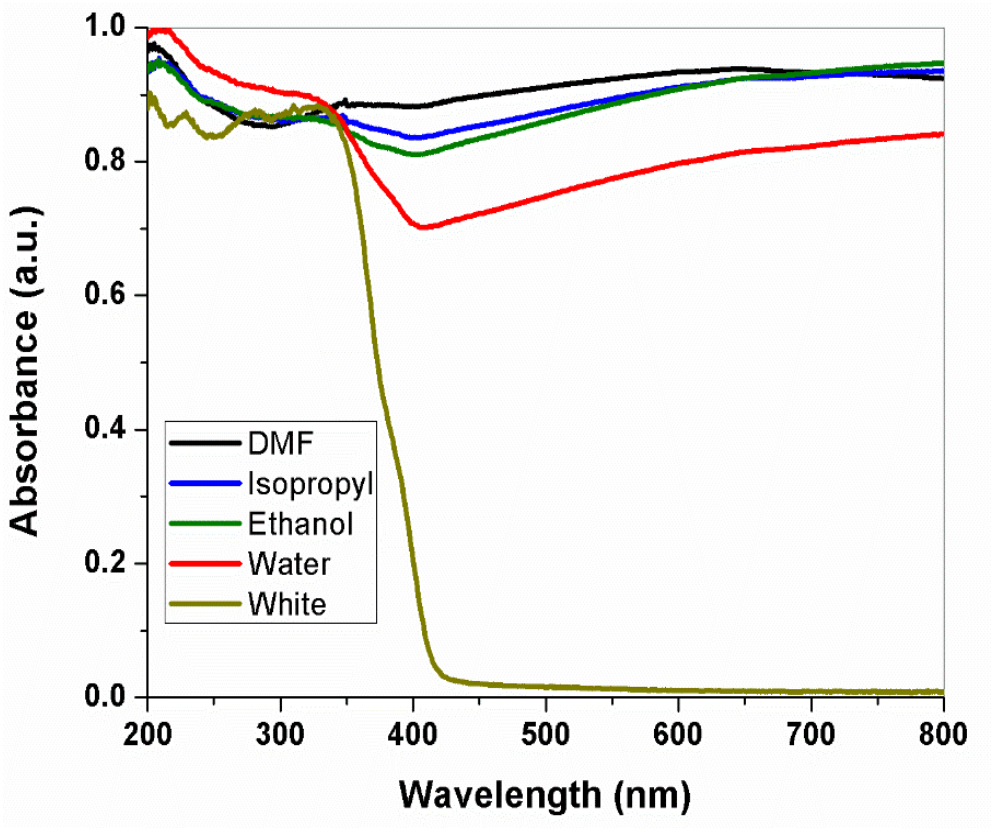

Figure 3. 23. Absorbance spectra of white TiO_2 and black TiO_2 synthetized in DMF, Ethanol and Isopropyl alcohol for 60 minutes of laser irradiation.

3.2.4.3 Bandgap analysis

To conclude with the optical characterizations, the estimation of band gap was achieved by Kubelka-Munk function method. The Kubelka-Munk function consists the equation and plotting (F(R)**hv*)1/n, n = 1/2 and 2 for direct and indirect band gaps vs *hv*.

$$F(R) = \frac{(1-R)^2}{2R} \qquad \textit{Eq. 3.7}$$

Figure 3.24 presents the estimate band gap for white TiO_2, which contains anatase in major composition thus indirect bandgap $(F(R)*hv)^{1/2}$, was estimated. On the other hand, water samples of 45, 60, 75, and 90 min present rutile phase in composition and direct band gap was estimated as is shown in Figure 2.25. In the same way, direct band gap

for DMF 60, ET 60 and ISO 60 were evaluated and are compared in Figure 3.26.

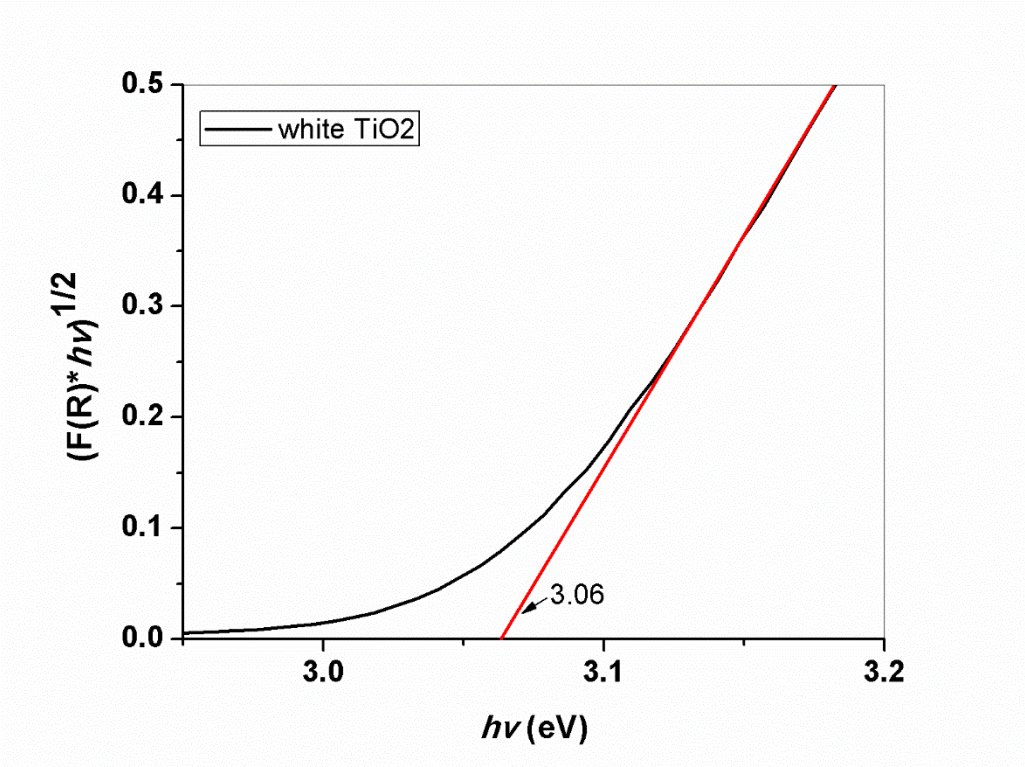

Figure 3. 24. Indirect band gap estimation of white TiO_2

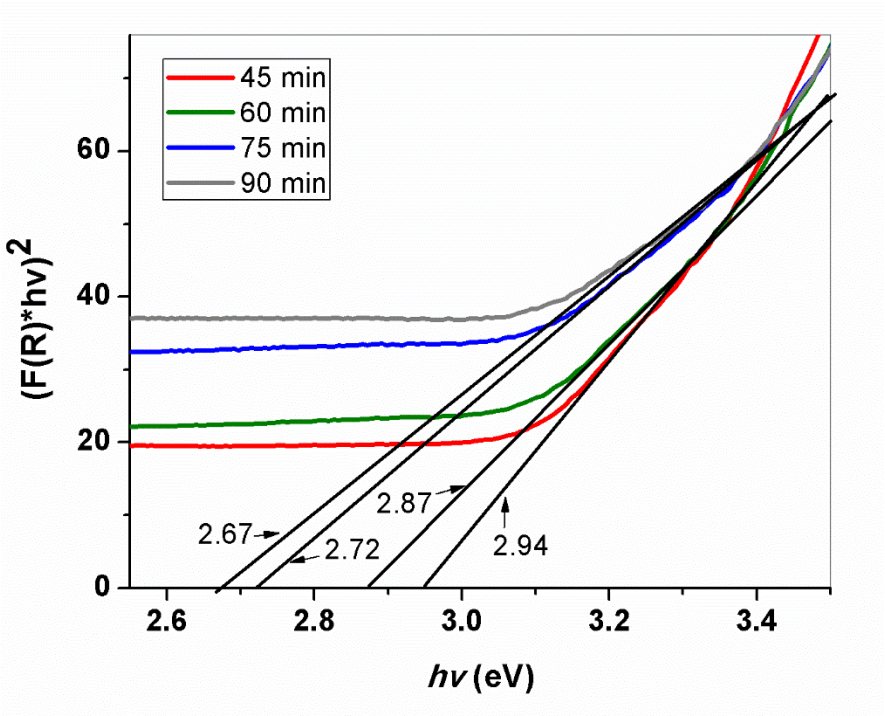

Figure 3. 25.Direct band gap estimation of black TiO_2 synthetized in water for 45, 60, 75 and 90 minutes of laser irradiation.

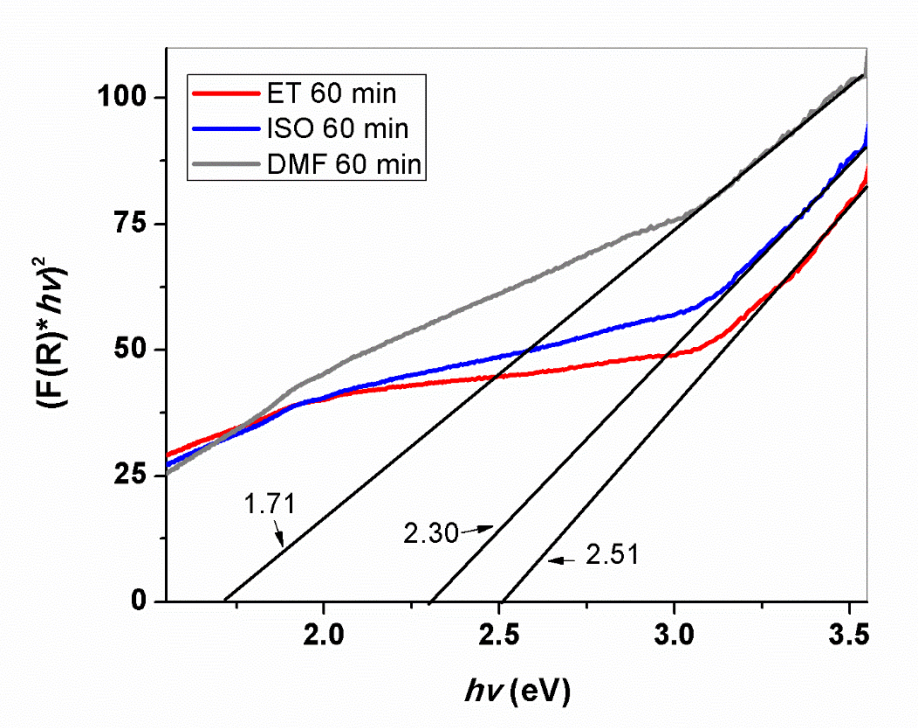

Figure 3. 26. Direct band gap estimation of black TiO_2 synthetized in ethanol, isopropyl alcohol and DMF for 60 minutes of laser irradiation.

3.2.5 Analysis of photocatalytic activity

The results obtained by photocatalytic analysis were achieved by the experiment set up shown in the Figure 3.27. The irradiation was carried out by a green LED at 523 nm, 10 W of power and Lumens of 1000mA located in the bottom of the photoreactor. The photocatalytic reaction was carried out for 1 hour for each sample and absorbance spectrum was reported every 10 minutes. The corresponded absorbance peak of rhodamine B is located at 553.5 nm as is shown in the absorbance spectrum of the photocatalytic activity of white TiO_2, Figure 3.26. During the photocatalytic process the absorbance peak slightly shift to blue, and a decreasing concentration of rhodamine B.

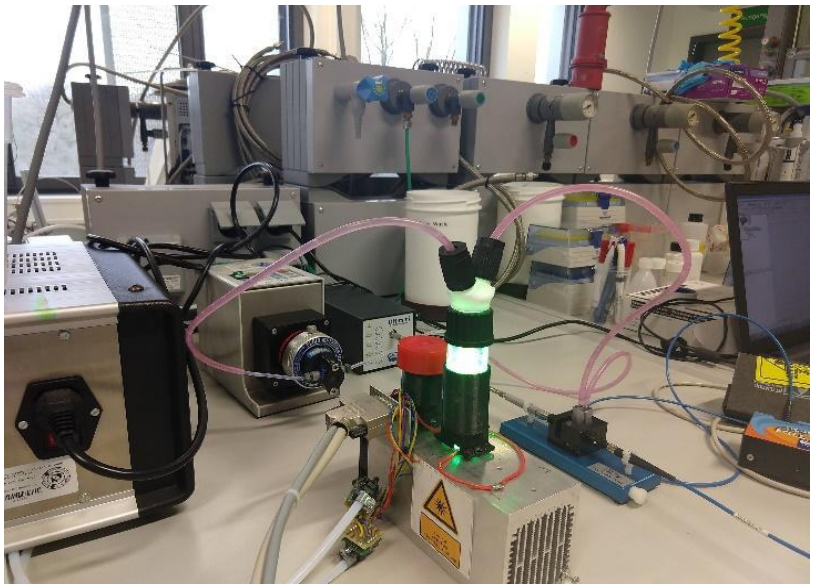

Figure 3. 27. Imagens of the experimental setup for photocatalytic tests.

The photocatalytic activity of synthesized black TiO_2 in water was examined and showed in Figure 3.28. The degradation of rhodamine B is observed for all samples, but significative decreasing of rhodamine B concentration was observed by the 90 min sample, Figure 3.29 (a). Besides, the shift to blue spectrum increased for all samples, by increasing irradiation time the samples have more photocatalytic activity

to degrade rhodamine B and to increase the shifting to blue as is shown in Figure 3.29 (d).

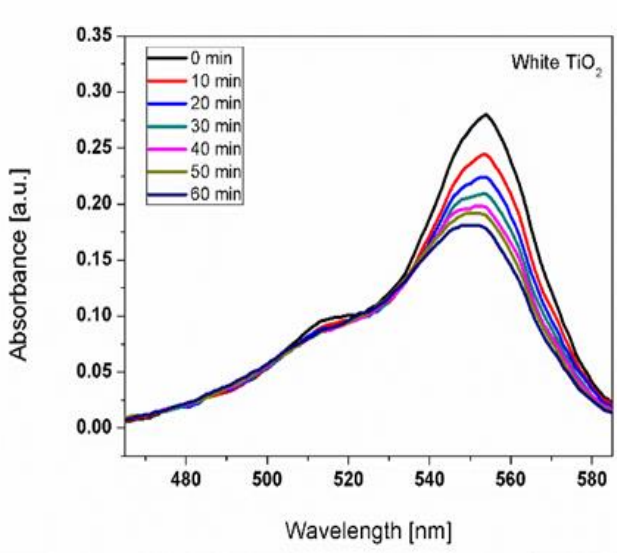

Figure 3. 28 Absorbance spectra of rhodamine B degradation with white TiO_2 as photocatalyst.

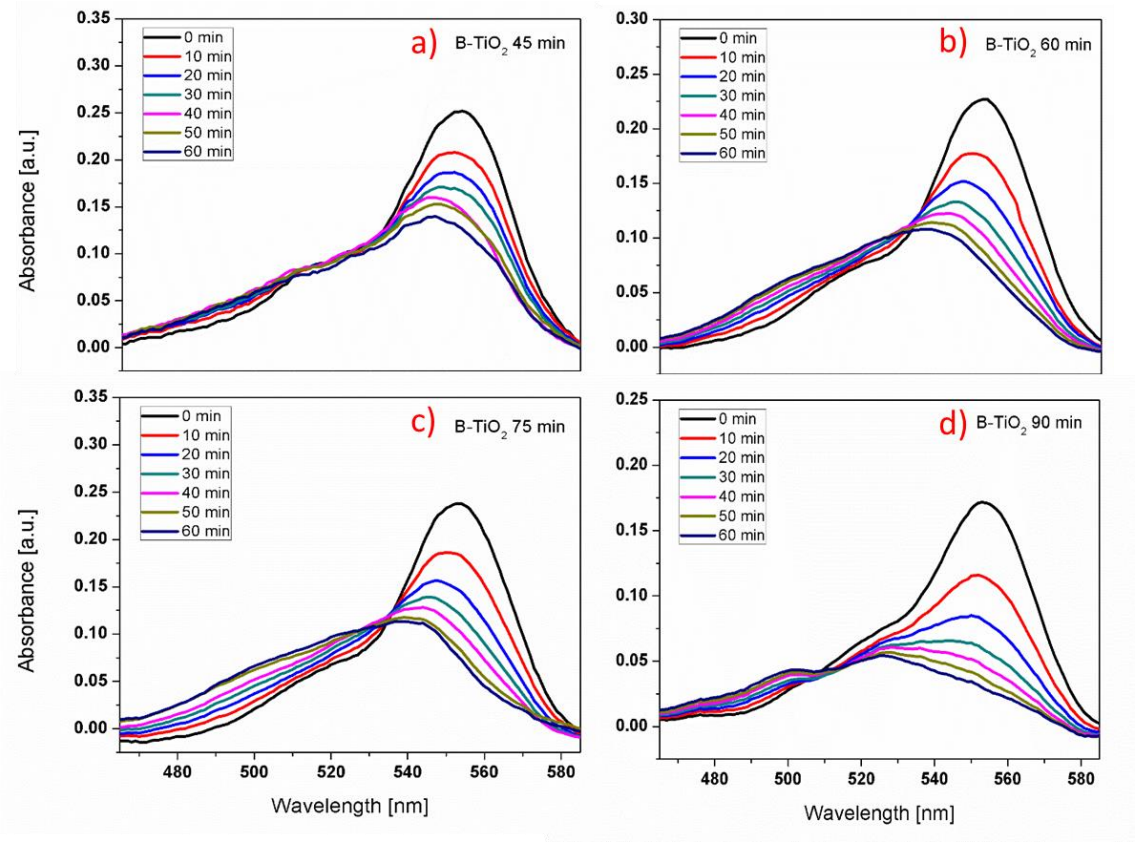

Figure 3. 29. Absorbance spectra of degradation of rhodamine B during white and black TiO_2 photocatalysis.

Besides, black TiO_2 at 60 and 75min samples showed slight difference in degradation ratio. In brief, the photocatalytic activity increases by increasing the time of irradiation in the synthesis of black TiO_2 due to the introduction of defects in the surface of the synthesized particles in water medium.

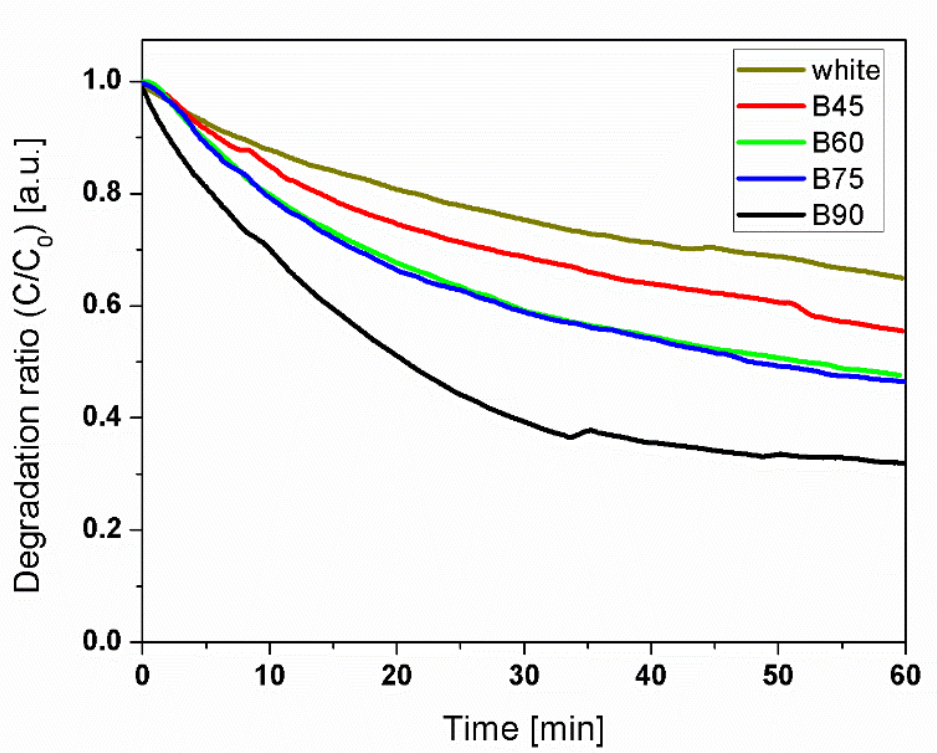

Figure 3. 30. Degradation ratio of rhodamine B vs Time of visible light irradiation. Comparation of different synthesized photocatalysts.

Likewise, results of photocatalytic activity of black TiO_2 in DMF, Isopropyl alcohol and ethanol solvents were compared with water and white TiO_2. Figure 3.31 shows the different absorbance spectra of the photocatalytic process for water 60 (Figure 3.31 (a)), ISO 60 (Figure 3.31 (b), ET 60 (Figure 3.31 (c)), and DMF 60 (Figure 3.32 (d)).

In resume, the photocatalytic activity and shift of the absorbance was also detected. The shift in absorbance spectrum of water 60 sample Figure 3.31 (a) shown a significant difference compared with ISO 60 (Figure 3.31 (b)), ET 60 (Figure 3.31 (c)) and DMF 60 (Figure 3.31 (d)), which presented slight shifting in the absorbance spectra. The obtention

of intermediary compounds that are not presents in the photocatalytic reactions of organic solvents media samples may be a reason of this shifting.

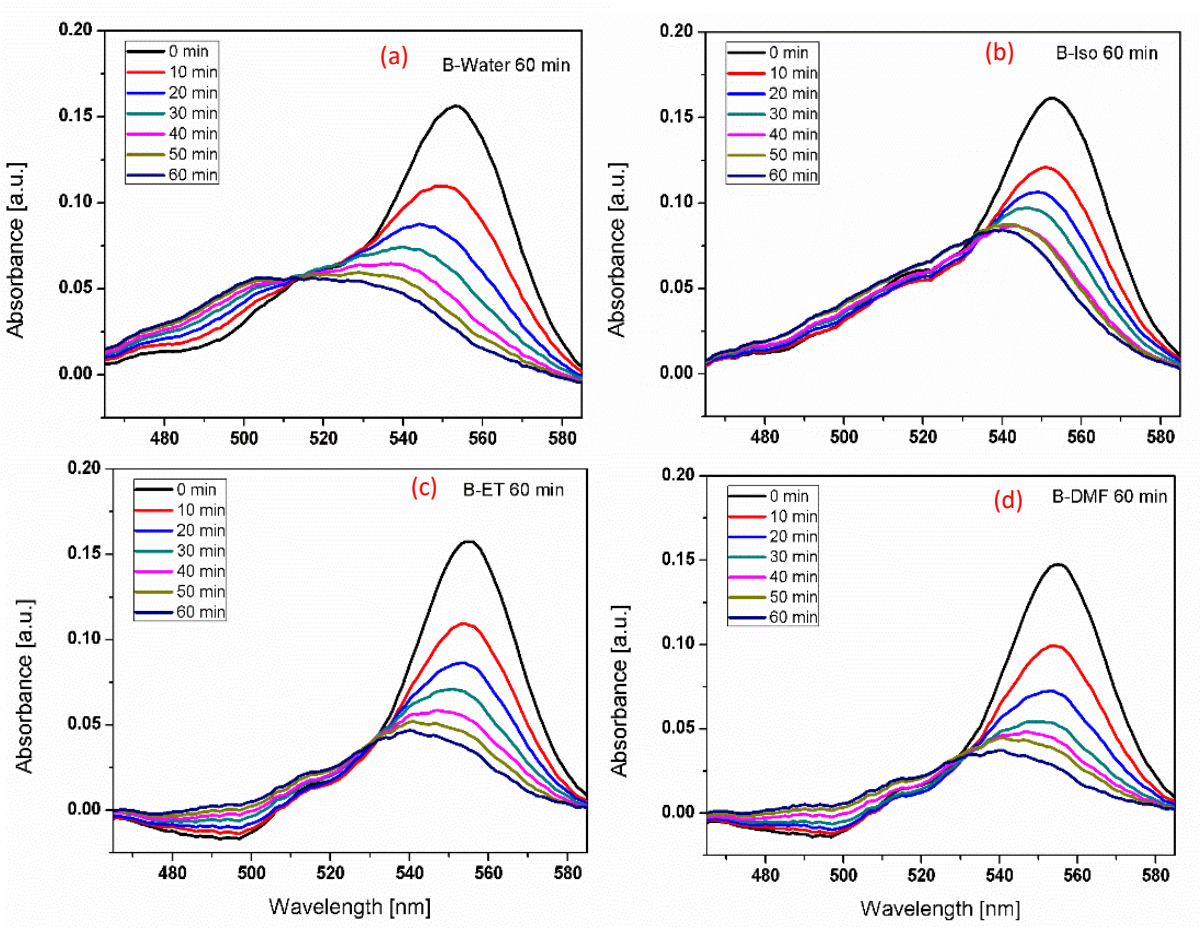

Figure 3. 31. Absorbance spectra of degradation of rhodamine B with black TiO_2 as photocatalyst. (a) Water-60 sample, (b) ISO 60 samples, (c) ET 60 sample and (d) DMF sample.

Certainly, photocatalytic activity is enhanced by the synthesis of black TiO_2 of organic solvents (DMF, isopropyl alcohol and ethanol), in Figure 3.32. The presence of carbon in the particles surface increased the visible light absorption since the photocatalytic reaction are carrying out in the surface.

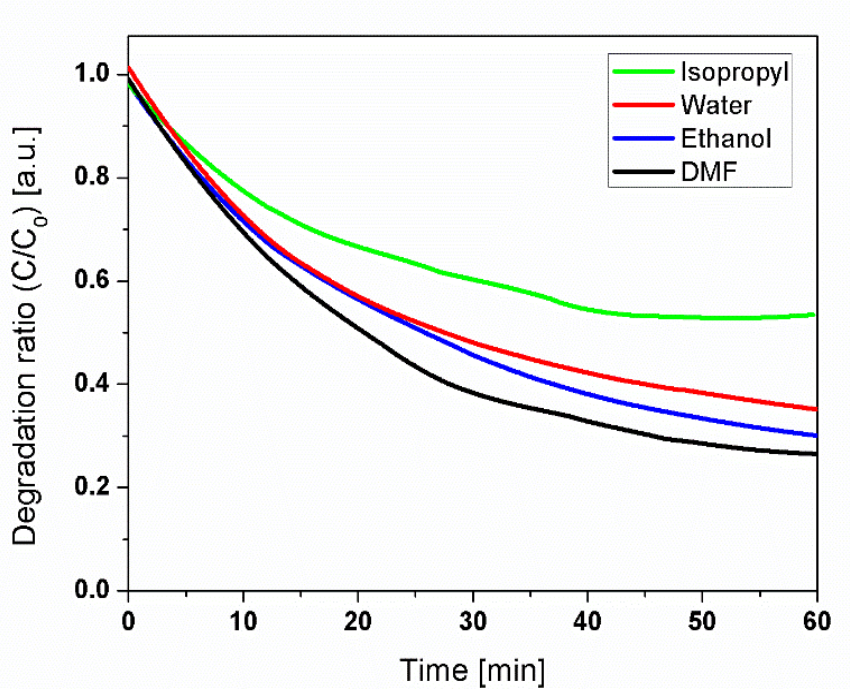

Figure 3. 32. Degradation ratio of rhodamine B vs time of visible light irradiation. Comparation of different synthesized photocatalysts.

Pulsed laser irradiation was successful to obtain black TiO_2 in different solvents. The different characterization techniques and their analysis confirmed the structure, morphology, composition and optical properties of white and black TiO_2. Photocatalytic properties of black TiO_2 nanoparticles under visible light irradiation showed an enhanced photocatalytic dye decay compared to the white TiO_2 nanomaterials.

CHAPTER 4

DISCUSSION AND CONCLUSIONS

4.1 Discussion

The synthesis of black TiO_2 in water was previously achieved by laser irradiation with a pico second laser pulsed at wavelength of 355 nm (UV), which possess a high energy and the light emission was supposed to be absorbed by TiO_2 since it absorbs in UV region. The synthesis of our nanomaterial was carried out by a pulsed nano second laser at 532 nm, what means the energy was relative lower compared to UV ps laser. In addition, studies shown that fluencies of 0.26 J/cm^2 were able to cause a heating effect in TiO_2 to transform anatase to rutile phase. The fluence for our experiments was 0.65 J/cm^2 which is considered high enough to produce this effect of heating and melting for those nanoparticles. The method of synthesis compared with sol-gel, hydrothermal methods, laser irradiation method resulted in an easy sample preparation and there are not residues after the synthesis.

The XRD results showed anatase to rutile transformation was achieved and the rutile phase composition increased by the increment of laser time irradiation. Those results are confirmed with other black TiO_2 nanomaterials. The synthesis in ethanol, isopropyl alcohol, and DMF solvents promote the rutile composition increment in (1 0 1) surface direction. Those surface directions were also observed to contribute to increase the photocatalytic activity. On the other hand, results in binding energy showed change in chemical states. Samples in DMF, isopropyl alcohol and ethanol showed more change in O1s binding energy due to the C-O groups presents in the solvents. The present of low concentration

of low oxygen present in the liquid media left oxygen vacancies showed in the elemental chemical mapping.

In contrast to previous reports, the synthesized black TiO_2 nanomaterial by this method allowed the melting, nucleation and growth of large particles, which is supposed to reduce the photocatalytic activity due to the reduction of surface of the material for the reactions. Instead of that, photocatalytic activity was enhanced, and it can be explained by the presence of smaller nanoparticles around the bigger particles obtained by laser fragmentation during the synthesis. It can contribute with the more active surface of reaction and bigger particles can work as supports.

The liquid media promoted change in morphology since depending on the nature of the media, the growth can be continuous or stopped during the synthesis process. The scope of this work brings the capacity to identify the principal phenomena for the obtention of black TiO_2 by this method.

4.2 Conclusions

The objectives of this work were fulfilled, thus the synthesis of black TiO_2 in water, isopropyl alcohol, ethanol and DMF was carried out under laser irradiation. The modification from white to black TiO_2 was observed and evaluated by the various characterization methods utilized in the study. The color change through irradiation time, different solvents, the evidence of oxygen vacancies, the present of amorphous nanomaterial, the anatase to rutile phase transition (XRD and Raman analysis), narrowing of band gap edge (band gap estimation, valence band analysis), and the effect in the morphology (SEM microscopy) through different liquid media and photocatalytic activity was observed.

The enhance of photocatalytic activity under visible irradiation was achieved due to the surface modification by the incorporation of defects

during the laser irradiation. The synthesis through organic solvents media leaves a carbon shell which improve the absorbance in the surface under visible light. The rate content increased by sample of more irradiated time. In case of the solvents media, the DMF resulted in the most photocatalytic activated sample.

4.3 Recommendations

For future investigation, the variation of the parameter for the synthesis could bring a better understanding of the phenomena which affected the properties of the nanoparticles. It can also contribute to the control of the particle size.

The synthesis of black TiO_2 by laser irradiation leads the advantage of the quantity material obtention compared to other methods of more the exploration for new application such as catalysis and solar cells. The study of the carbon shell formed by the synthesis of nanomaterial in organic solvents is another topic to attend in detail.

REFERENCES

[1] X. Chen, S.S. Mao, Titanium dioxide nanomaterials: synthesis, properties, modifications, and applications, Chem. Rev. 107 (2007) 2891–2959.

[2] R. Daghrir, P. Drogui, D. Robert, Modified TiO2 for environmental photocatalytic applications: a review, Ind. Eng. Chem. Res. 52 (2013) 3581–3599.

[3] A. Fujishima, K. Honda, Electrochemical photolysis of water at a semiconductor electrode, Nature 238 (1972) 37.

[4] X. Chen, D. Zhao, K. Liu, C. Wang, L. Liu, B. Li, Z. Zhang, D. Shen, Laser-modified black titanium oxide nanospheres and their photocatalytic activities under visible light, ACS Appl. Mater. Interfaces 7 (2015) 16070–16077.

[5] X. Chen, L. Liu, F. Huang, Black titanium dioxide (TiO2) nanomaterials, Chem. Soc. Rev. 44 (2015) 1861–1885.

[6] C. Fan, C. Chen, J. Wang, X. Fu, Z. Ren, G. Qian, Z. Wang, Black hydroxylated titanium dioxide prepared via ultrasonication with enhanced photocatalytic activity, Sci. Rep. 5 (2015) 11712.

[7] L. Yan, T. Lihong, T. Xinyu, L. Xin, C. Xiaobo, Synthesis, properties, and applications of black titanium dioxide nanomaterials, Sci. Bull. 62 (2017) 431.

[8] U.I. Gaya, A.H. Abdullah, Heterogeneous photocatalytic degradation of organic contaminants over titanium dioxide: a review of fundamentals, progress and problems, J Photochem Photobiol C: Photochem Rev 9 (2008) 1–12.

[9] M. Pelaez, N.T. Nolan, S.C. Pillai, M.K. Seery, P. Falaras, A.G. Kontos, P.S.M. Dunlop, J.W.J. Hamilton, J.A. Byrne, K. O'Shea, M.H. Entezari, D.D. Dionysiou, A review on the visible light active titanium dioxide photocatalysts for environmental applications, Appl. Catal. B Environ. 125 (2012) 331–349.

[10] H. Park, Y. Park, W. Kim, W. Choi, Surface modification of TiO2 photocatalyst for environmental applications, J Photochem Photobiol C: Photochem Rev 15 (2013) 1–20.

[11] https://www.usgs.gov/centers/nmic/titanium-statistics-and-information

[12] J.L. Murray, The O-Ti (Oxygen-Titanium) System, Bulletin of Alloy Phase Diagrams Vol. 8 No. 2 1987

[13] B. Predel, Landolt-Börnstein New Series IV/5-I, (Springer-Berlag, Berlin Heidelberg-New York, 1998, p.92)

[14] W. Ma, Z. Lu, M. Zhang, Investigation of structural transformations in nanophase titanium dioxide by Raman spectroscopy, Appl. Phys. A 66 (1998) 621

[15] L. S. Dubrovinsky, N. A. Dubrovinskaia, V. Swamy, J. Muscat, N. M. Harrison, R. Ahuja, B. Holm, B. Johansson, The hardest known oxide, Nature 410 (2001) 653

[16] Tesis doctoral, R. Portela Rodríguez, Eliminación fotocatalítica de H2S en aire mediante TiO2 soportado sobre sustratos transparentes en el UV-A, Universidad de Santiago de Compostela, 2008

[17] S. Girish Kumar and K. S. R. Koteswara Rao, Polymorphic phase transition among the titania crystal structures using a solution-based approach: from precursor chemistry to nucleation process, Nanoscale, 2014, 6, 11574

[18] N. Satoh, T. Nakashima, K. Yamamoto, Metastability of anatase: size dependent and irreversible anatase-rutile phase transition in atomic-level precise titania, SCIENTIFIC REPORTS, 3: 1959, DOI:10.1038/srep01959

[19] Deskins, N. A., Worcester Polytechnic Institute, First Principles Modeling of TiO2 Rutile/Anatase Interfaces, AIChE Annual Meeting

[20] W. Jun Kim, M. Hoon Han, S. Lebègue, E. Kyun Lee, H. Kim, Electronic Structure and Band Alignments of various phases of Titania using the self-consistent Hybrid Density Functional and DFT+UMethods

[21] D. O. Scanlon, C. W. Dunnill, J. Buckeridge, S. A. Shevlin, Band alignment of rutile and anatase TiO2

[22] T. Luttrell, S. Halpegamage, J. Tao, A. Kramer et. al., Why is anatase a better photocatalyst than rutile? - Model studies on epitaxial TiO2 films, Sci Rep. 2014; 4: 4043

[23] X. Chen, L. Liu, Peter Y. Yu, Samuel S., Increasing Solar Absorption for Photocatalysis with Black Hydrogenated Titanium Dioxide Nanocrystals, Science 331, 746 (2011)

[24] M. Tian, M. Mahjouri-Samani, G. Eres, R. Sachan, M. Yoon, M.F. Chisholm, K. Wang, A.A. Puretzky, C.M. Rouleau, D.B. Geohegan, G. Duscher, Structure and formation mechanism of black TiO2 nanoparticles, ACS Nano 9 (2015) 10482–10488.

[25] K. Zhang, J.H. Park, Surface localization of defects in black TiO2: enhancing photoactivity or reactivity, J. Phys. Chem. Lett. 8 (2017) 199–207.

https://www.nature.com/articles/srep11482

[26] Teh, C. M.; Mohamed, A. R. Role of titanium dioxide and iondoped titanium dioxide on phtotocatalytic degradation of organic pollutants (phenol compounds and dyes) in aqueous solutions: A review. J. Alloys Compd. 2011, 509, 1648−1660.

[27] Yoon, J. W.; Sasaki, T.; Koshizaki, N. Dispersion of nanosized noble metals in TiO2 matrix and their photoelectrode properties. Thin Solid Films 2005, 483, 276−282.

[28] Kment, S.; Kmentova, H.; Kluson, P.; Krysa, J.; Hubicka, Z.; Cirkva, V.; Gregora, I.; Solcova, O.; Jastrabik, L. Notes on the photoinduced characteristics of transition metal-doped and undoped titanium dioxide thin films. J. Colloid Interface Sci. 2010, 348, 198−205.

[29] Li, H.; Wang, D.; Wang, P.; Fan, H.; Xie, T. Synthesis and studies of the visible light photocatalytic properties of near monodisperse Bi-doped TiO2 nanospheres. Chem. Eur. J. 2009, 15, 12521−12527.

[30] Asahi, R.; Morikawa, T.; Ohwaki, T.; Aoki, K.; Taga, Y. Visible light photocatalysis in nitrogen-doped titanium oxides. Science 2001, 293 (5528), 269−271.
[31] Rehman, S.; Ullah, R.; Butt, A. M.; Gohar, N. D. Strategies of making TiO2 and ZnO visible light active. J. Hazard. Mater. 2009, 170, 560−569.
[32] Chen, X. B.; Liu, L.; Liu, Z.; Marcus, M. A.; Wang, W. C.; Oyler, N. A.; Grass, M. E.; Mao, B.; Glans, P. A.; Yu, P. Y.; Guo, J.; Mao, S. S.Properties of Disorder-Engineered Black Titanium Dioxide Nanoparticles Through Hydrogenation. Sci. Rep. 2013, 3, 1510.
[33] Liu, L.; Yu, P. P.; Chen, X.; Mao, S. S.; Shen, D. Z. Hydrogenation and Disorder in Engineered Black TiO2. Phys. Rev. Lett. 2013, 111, 065505.
[34] A. Pérez del Pino, Coloración del titanio mediante el tratamiento superficial de oxidación por láser, Tesis Doctoral - Departamento - Física Aplicada i Òptica, Barcelona 2003

[35] G.G. Guillén, S. Shaji, M.I.M. Palma, D. Avellaneda, G.A. Castillo, T.K.D. Roy, D.I.G. Gutiérrez, B. Krishnan, Effects of ablation energy and post irradiation on the structure and properties of titanium dioxide nanomaterials, Appl. Surf. Sci. 405 (2017) 183–194.

[36] H. Zhang, J.F. Banfield, Phase transformation of nanocrystalline anatase-to-rutile via combined interface and surface nucleation, J. Mater. Res. 15 (2000) 437–448.